

## RESEARCH ARTICLE

10.1002/2017JD027260

## Key Points:

- We validate regional climate simulations of  $\delta D$  in European precipitation and water vapor
- We quantify the impact of fractionation processes by means of sensitivity runs
- Rainout, evapotranspiration, and subcloud processes control European  $\delta D$  to a similar extent

## Supporting Information:

- Supporting Information S1

## Correspondence to:

E. Christner,  
emanuel.christner@kit.edu

## Citation:

Christner, E., Aemisegger, F., Pfahl, S., Werner, M., Cauquoin, A., Schneider, M., et al. (2018). The climatological impacts of continental surface evaporation, rainout, and subcloud processes on  $\delta D$  of water vapor and precipitation in Europe. *Journal of Geophysical Research: Atmospheres*, 123, 4390–4409. <https://doi.org/10.1002/2017JD027260>





Received 7 JUN 2017

Accepted 19 FEB 2018

Accepted article online 23 FEB 2018

Published online 26 APR 2018

## The Climatological Impacts of Continental Surface Evaporation, Rainout, and Subcloud Processes on $\delta D$ of Water Vapor and Precipitation in Europe

Emanuel Christner<sup>1</sup> , Franziska Aemisegger<sup>2,3</sup>, Stephan Pfahl<sup>3</sup> , Martin Werner<sup>4</sup> , Alexandre Cauquoin<sup>4</sup> , Matthias Schneider<sup>5</sup>, Frank Hase<sup>5</sup>, Sabine Barthlott<sup>5</sup>, and Gerd Schädler<sup>1</sup>

<sup>1</sup>Institute of Meteorology and Climate Research-Department Troposphere Research (IMK-TRO), Karlsruhe Institute of Technology, Karlsruhe, Germany, <sup>2</sup>Centre for Environmental and Climate Research, Lund University, Lund, Sweden, <sup>3</sup>Institute for Atmospheric and Climate Science, ETH Zurich, Zurich, Switzerland, <sup>4</sup>Alfred Wegener Institute, Helmholtz Centre for Polar and Marine Research, Division, Climate Science–Paleoclimate Dynamics, Bremerhaven, Germany, <sup>5</sup>Institute of Meteorology and Climate Research-Department Atmospheric Trace Gases and Remote Sensing (IMK-ASF), Karlsruhe Institute of Technology, Karlsruhe, Germany

**Abstract** All types of applications of stable water isotopes, for example, for the reconstruction of paleotemperatures or for climate model validation, rely on a proper understanding of the mechanisms determining the isotopic composition of water vapor and precipitation. In this study, we use the isotope-enabled limited-area model COSMO<sub>iso</sub> to characterize the impacts of continental evapotranspiration, rainout, and subcloud processes on  $\delta D$  of European water vapor and precipitation. To this end, we first confirm a reliable implementation of the most important isotope fractionation processes in COSMO<sub>iso</sub> by comparing 5 years of modeled  $\delta D$  values with multiplatform  $\delta D$  observations from Europe (remote sensing observations of the  $\delta D$  of water vapor around 2.6 km above ground level, in situ  $\delta D$  measurements in near-surface water vapor, and  $\delta D$  precipitation data from the Global Network of Isotopes in Precipitation). Based on six 15 year sensitivity simulations, we then quantify the climatological impacts of the different fractionation processes on the  $\delta D$  values. We find  $\delta D$  of European water vapor and precipitation to be most strongly controlled by rainout. Superimposed to this are the effect of subcloud processes, which especially affects  $\delta D$  in precipitation under warm conditions, and the effect of continental evapotranspiration, which exerts an important control over the  $\delta D$  of near-surface water vapor. In future studies, the validated COSMO<sub>iso</sub> model can be employed in a similar way for a comprehensive interpretation of European isotope records from climatologically different time periods.

### 1. Introduction

Stable isotopes of atmospheric water are fractionated during phase changes, making the isotopic composition of water sensitive to a wide range of effects such as surface evaporation (Craig & Gordon, 1965; Pfahl & Wernli, 2009; Zhang et al., 2010), rainout (Blossey et al., 2010; Jouzel, 1986; Jouzel & Merlivat, 1984), and postcondensational isotope exchange below the cloud base (Friedman et al., 1962; Gedzelman & Arnold, 1994; Stewart, 1975). For this reason, the isotopic composition of precipitation or water vapor is a useful and widely employed proxy for constraining processes in the paleoclimatic or modern hydrological cycle (Dansgaard, 1964; Dansgaard et al., 1969; Gat, 1996).

Since 1961, isotope concentration ratios in precipitation such as  $R_D = [HD^{16}O]/[H_2^{16}O]$  have been analyzed at more than 800 meteorological stations around the world within the Global Network of Isotopes in Precipitation (GNIP) of the International Atomic Energy Agency and the World Meteorology Organization (IAEA/WMO, 2016). Because of the small abundances of  $HD^{16}O$ ,  $R_D$  is commonly referred to as  $\delta D = R_D/R_{D,VSMOW2} - 1$ , with  $R_{D,VSMOW2} = 0.00031152$  (IAEA, 2009) (see Coplen, 2011, for details). A major finding from the GNIP data is a general relation between the degree of rainout of air masses and  $\delta D$ , resulting from fractionation processes that favor the presence of heavy isotopes in the condensed phase. This relation, in turn, results in typical spatial patterns of  $\delta D$  in precipitation such as a decrease of  $\delta D$  values over continents with distance

to the coast ("continental effect"), a decrease toward high latitudes ("latitude effect"), and lower  $\delta D$  values at elevated locations ("altitude effect") (Araguas et al., 1996; Dansgaard, 1964; Yoshimura, 2015).

A number of applications are based on this relation between the degree of rainout of air masses and isotope ratios: For example, hydrological studies use the seasonality and altitude dependence of isotope ratios in precipitation for the investigation of ground water formation (de Vries & Simmers, 2002). In paleoresearch, isotope ratios in archives such as ice cores (e.g., Dansgaard et al., 1969; Masson-Delmotte et al., 2005) or speleothems (e.g., Boch et al., 2011; Wang, 2001) are used for reconstructing temperature or precipitation amounts of the past. The interpretation of isotope signals is, however, often challenging because not only rainout but also moisture uptake from surface evaporation (e.g., Jacob & Sonntag, 1991) and fractionating isotope exchange between falling precipitation and water vapor (e.g., Friedman et al., 1962; Gedzelman & Arnold, 1994; Stewart, 1975) modify the isotope ratios. For this reason, the different isotope applications require a detailed knowledge about the impact of processes which are archived by water isotopes in a certain region.

Sensitivity experiments with isotope-enabled atmospheric general circulation models (GCMs) provide a good framework for separating the impacts of different fractionation processes and for quantitatively understanding isotope signals: For instance, Field et al. (2010) analyzed the effect of postcondensation isotope exchange between raindrops and water vapor at different latitudes with the "GCM ModelE" of the Goddard Institute for Space Studies. Aemisegger et al. (2015) investigated the impact of below-cloud effects and evapotranspiration during a cold front passage in Switzerland with the regional model COSMO<sub>iso</sub>. Dütsch et al. (2016) used the same model to study effects of in- and below-cloud fractionation as well as moisture advection in an idealized midlatitude cyclone. Risi et al. (2016) evaluated the role of isotope fractionation during continental surface evaporation with the coupled LMDZiso-ORCHIDEEiso GCM. In addition to these models, a still increasing number of further GCMs exist that are equipped with stable isotope physics and which consequently are suited for similar sensitivity experiments.

Most of the isotope-enabled models were validated against GNIP observations (e.g., Hoffmann et al., 1998; Joussaume et al., 1984; Jouzel et al., 2000), justifying some confidence in a reliable representation of isotope fractionation in the models. However, because GNIP data reflect the integrated fractionation history of precipitating air masses, an exclusive validation against GNIP data does not allow to finally rule out potentially compensating model errors related to different fractionation processes. For this reason, quantifying the impact and role of different fractionation processes with such models remains a challenge.

In this context, observations of the isotopic composition of water vapor allow for a complementary validation of the modeled  $\delta D$  of water vapor at different points in time, before the formation of precipitation. For a long time, only a few studies with  $\delta D$  measurements in water vapor existed, which were based on different time-consuming water vapor trapping techniques, limiting observations to a few case studies (e.g., Jacob & Sonntag, 1991; Schoch-Fischer et al., 1983; Taylor, 1984). In recent years, advances in laser spectroscopy techniques have enabled continuous monitoring of  $\delta D$  of water vapor, leading to a substantially increased number of  $\delta D$  observations in near-surface water vapor, which allowed for more extensive investigations of isotope fractionation during surface evaporation (e.g., Aemisegger et al., 2012; Noone et al., 2011; Steen-Larsen et al., 2014). In addition, ground-based (Rokotyan et al., 2014; Schneider et al., 2012) as well as satellite-based (e.g., Frankenberg et al., 2009; Schneider & Hase, 2011; Worden et al., 2006) remote sensing observations of  $\delta D$  of water vapor in the free troposphere became available.

Several studies already made use of the newly available multiplatform  $\delta D$  observations for validating isotope-enabled GCMs. For instance, Frankenberg et al. (2009) compared IsoGSM simulations with satellite-based  $\delta D$  total column measurements from SCIAMACHY (SCanning Imaging Absorption SpectroMeter for Atmospheric CHartographY). Field et al. (2010) compared GISS ModelE simulations with observations of  $\delta D$  of free tropospheric water vapor from the satellite-based TES (Tropospheric Emission Spectrometer) and in situ  $\delta D$  observations from Hawaii. Werner et al. (2011) compared ECHAM5-wiso simulations with in situ measurements of  $\delta D$  of near-surface water vapor and SCIAMACHY observations. Risi et al. (2012a) evaluated LMDZiso simulations with different satellite-based and ground-based remote sensing observations of  $\delta D$  of free tropospheric and lower stratospheric water vapor and a couple of ground-based and airborne in situ measurements. Common to these validation studies is that long-term averages of simulations have been compared to long-term averages of observations. The representativeness of the model-data comparison regarding, for instance, different synoptic conditions is therefore limited. In addition, the comparability of

isotope observations and simulations is reduced, considering the coarse spatial resolution ( $>1^\circ \times 1^\circ$ ) of the employed GCMs.

The objective of this paper is to compare multiplatform  $\delta D$  observations with medium-resolution simulations ( $0.5^\circ \times 0.5^\circ$ ) of the isotope-enabled limited-area model COSMO<sub>iso</sub> on a 3-hourly time scale. In a second step, we use the validated COSMO<sub>iso</sub> for disentangling the most important fractionation processes controlling  $\delta D$ . As a target region for our regional simulations we chose Europe for two reasons: First, a number of different fractionation processes (rainout, evapotranspiration, subcloud processes) are expected to play an important role in Europe (Aemisegger et al., 2015), making an attribution of  $\delta D$  to different fractionation processes particularly valuable. Second, for Karlsruhe in central Europe a set of observations of  $\delta D$  of near-surface water vapor and  $\delta D$  of lower tropospheric water vapor from the MUSICA (MULTi-platform remote Sensing of Isotopologues for investigating the Cycle of Atmospheric water) framework (Schneider et al., 2012) exists, which we combine with extensive GNIP data available for Europe. In section 2, we describe the model setup of COSMO<sub>iso</sub> and the used multiplatform  $\delta D$  observations (GNIP observations, in situ measurements of  $\delta D$  of near-surface water vapor, and ground-based remote sensing observations of  $\delta D$  of free tropospheric water vapor). In section 3, we confirm the reliable implementation of the most important fractionation processes in COSMO<sub>iso</sub> by comparing simulations for Europe with the multiplatform  $\delta D$  observations. In section 4, we use sensitivity runs of the validated COSMO<sub>iso</sub> to quantify the impacts of different fractionation processes on  $\delta D$ .

## 2. Methods

### 2.1. COSMO<sub>iso</sub>

#### 2.1.1. Model Description

The isotope-enabled limited-area model COSMO<sub>iso</sub> (Pfahl et al., 2012) is an extended version of the numerical weather prediction model COSMO (Steppeler et al., 2003) (version 4.18), which is capable of explicitly simulating the stable water isotopes  $H_2^{16}O$ ,  $HD^{16}O$ , and  $H_2^{18}O$ . Since few  $H_2^{18}O$  observations from the free troposphere exist, we focus in this paper only on  $\delta D$ . Because investigated time periods cover several years, we operated COSMO<sub>iso</sub> in CLimate Mode, in which additional climatologically relevant parameters such as deep soil temperature are prognostically calculated (Rockel et al., 2008). When performing an isotope-enabled climate simulation over Europe, it is important to include a detailed description of isotope processes in the soil using a multilayer soil model. In particular in summer, a strong recycling contribution from evapotranspiration to central European precipitation (Sodemann & Zubler, 2010) and near-surface water vapor (Aemisegger et al., 2014) can be expected. The upper layer soil water enrichment can be important compared to deeper soil layers thus impacting the near-surface water vapor isotope composition through soil evaporation. To take such effects into account, we used the isotope-enabled version TERRA<sub>iso</sub> V.1 (Dütsch, 2017) of the multilayer soil module TERRA-ML (Schrodin & Heise, 2001). For more details regarding TERRA<sub>iso</sub> see supporting information and references cited therein (Barnes & Allison, 1983; Craig & Gordon, 1965; Doms et al., 1974; Dongmann et al., 1974; Dütsch, 2017; Farquhar & Cernusak, 2005; Harwood et al., 1999; Majoube, 1971a, 1971b; Mathieu & Bariac, 1996; Merlivat, 1978; Richards, 1931; Riley et al., 2002; Schrodin & Heise, 2001; Steppeler et al., 2003; Wang et al., 2012; Washburn & Smith, 1934).

#### 2.1.2. Simulation Setup

The COSMO<sub>iso</sub> simulations in this study are based on a horizontal resolution of  $0.5^\circ \times 0.5^\circ$  (in rotated coordinates, corresponding to  $55 \text{ km} \times 55 \text{ km}$ ), 50 hybrid vertical atmospheric layers, and 8 soil layers at depths of 0.005, 0.02, 0.06, 0.18, 0.54, 1.62, 4.86, and 14.58 m. Numerical time integration with an internal time step of 120 s was performed using a third-order Runge-Kutta scheme. Initial model data and data at the lateral boundaries (including water isotopes) of COSMO<sub>iso</sub> were derived from an isotope-enabled ECHAM5.4-wiso (Werner et al., 2011) simulation from 1 January 2000 to 31 December 2014 that had been nudged toward reanalysis dynamical fields. This ECHAM-wiso data are available every 12 h at a spectral resolution of T106 and on 31 vertical levels. The COSMO<sub>iso</sub> model domain was centered over Europe (Figure 1). In addition, the domain included large parts of the North Atlantic to ensure that most moisture source regions of European precipitation and water vapor are located within the model area and consequently isotope ratios are mainly determined by the isotope physics of COSMO<sub>iso</sub> and not by the boundary data. Because atmospheric fields and soil variables (temperature, soil water content, and  $\delta D$ ) were physically consistently initialized based on the ECHAM-wiso data, no spin-up time was considered for our COSMO<sub>iso</sub> simulations.

For validating COSMO<sub>iso</sub> against  $\delta D$  observations, we performed a COSMO<sub>iso</sub> reference simulation (EXP1). To optimize temporal agreement between  $\delta D$  variations in EXP1 and  $\delta D$  observations, horizontal wind fields

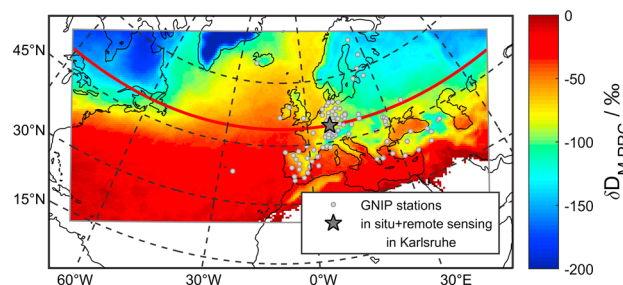


**Figure 1.** COSMO<sub>150</sub> model domain. Color code: modeled  $\delta D_{M,PRC}$  in precipitation in winters (December–January–February) from 2010 to 2014 (EXP1); open circles: GNIP stations; star: measurement site (Karlsruhe, Germany) for the in situ observations of  $\delta D$  in near-surface water vapor and the ground-based remote sensing observations of  $\delta D$  around 2.6 km above ground level; red line: vertical transect shown in Figure 3; white pixels within the model domain: modeled precipitation amount is smaller than 1 mm/month for more than 80% of the used months. GNIP = Global Network of Isotopes in Precipitation.

above the 850 hPa level in EXP1 were spectrally nudged (von Storch et al., 2000) toward the reanalysis-based dynamical fields of ECHAM-wiso. As the spectral nudging of horizontal wind fields increased the computation time by a factor of 4, we restricted the simulation period of EXP1 to 1 January 2010 to 31 December 2014. This time period covers in situ  $\delta D$  observations from Karlsruhe in central Europe, which were performed from 2012 to 2013, as well as 5 years of  $\delta D$  remote sensing observations at Karlsruhe, which have been performed since 2010.

### 2.1.3. Sensitivity Simulations

Based on six sensitivity simulations (Table 1), we assessed (1) the total sensitivity of the modeled  $\delta D$  to isotope fractionation processes in the atmosphere and the single sensitivities to (2) conditions at the ocean surface, (3) continental evapotranspiration, (4) subcloud processes, (5) rainout, and (6)  $\delta D$  provided at the lateral model boundaries. The simulation setup of the sensitivity runs with respect to model resolution and boundary data was the same as in EXP1. To derive more climatological information than from EXP1, we used a more extended 15 year simulation period from 1

January 2000 to 31 December 2014 for the sensitivity runs. Because of the high computational costs of the spectral nudging of horizontal wind fields, we did not apply the spectral nudging of wind fields in the climatological 15 year sensitivity runs. Figure 2a/2b shows mean differences between the nudged (EXP1) and a free-running (EXP2) simulation. For central European  $\delta D$  in winter precipitation there is a significant difference of about 5‰ between both simulations. This deviation is small compared to the absolute values of  $\delta D$  in precipitation and the magnitudes of sensitivities to be investigated in this paper. The difference between the nudged and the free-running simulation will thus be ignored in the discussion of the results.

1.  $S_{TOT}$ : Isotope fractionation during evaporation from the ocean marks the first phase change of water entering the atmospheric branch of the hydrological cycle. The impact of the fractionation processes 3–5 acting on atmospheric water vapor after evaporation from the ocean is quantified by the sensitivity  $S_{TOT}$ . From a Lagrangian perspective, the exact  $S_{TOT,exact,i}$  of water vapor with  $\delta D_i$  in a specific air parcel  $i$  sums up the changes of  $\delta D$  along the air parcel's trajectory after export from the marine boundary layer, where the isotopic composition of the air parcel was  $\delta D_{MBL,i}$ :  $S_{TOT,exact,i} = \delta D_i - \delta D_{MBL,i}$ . Similar to this,  $S_{TOT,exact,i}$  of a precipitation sample quantifies the changes of  $\delta D$  along the trajectory of the precipitating air parcel superimposed by the additional fractionation during the final formation of the sampled precipitation. For determining the average  $S_{TOT,exact}$  of a simulation, it would be necessary to calculate an extensive set of backward trajectories because  $\delta D_{MBL,i}$  for each air parcel would be needed. For reasons of simplicity and because variations of  $\delta D_{MBL,i}$  are relatively small (Benetti et al., 2014; Pfahl & Wernli, 2009; Steen-Larsen et al., 2014) compared to  $S_{TOT}$  in central Europe, we do not explicitly consider variations of  $\delta D_{MBL,i}$ . Instead, we assume a constant  $\delta D_{MBL} = -90\text{‰}$ , which is a typical model value of water vapor in the marine boundary layer at about 50°N (Figure 3). To determine  $S_{TOT}$ , we then calculate differences between the  $\delta D$  of precipitation or water vapor from EXP2 and  $\delta D_{MBL}$ :  $S_{TOT} = (\delta D \text{ from EXP2}) - \delta D_{MBL}$ .
2.  $S_{SST}$ : To assess the sensitivity of the modeled  $\delta D$  to conditions at the ocean surface ( $S_{SST}$ ), we decreased sea surface temperature (SST) by 3 K in the model run EXP3. The lower SST changed the strength of isotope fractionation during evaporation as well as moisture and energy fluxes at the ocean surface. In addition, the changed moisture and energy fluxes from the ocean also led to altered climatic conditions over the continent.  $S_{SST}$  was derived as  $(\delta D \text{ from EXP3}) - (\delta D \text{ from EXP2})$ .
3.  $S_{ET}$ : Various processes in the soil and close to the ground influence  $\delta D$  of moisture from continental evapotranspiration ( $\delta D_{ET}$ ) and consequently the  $\delta D$  of atmospheric water (see supporting information). To quantify the impact of continental evapotranspiration on atmospheric  $\delta D$ , we performed the sensitivity run EXP4, in which the effect of continental evapotranspiration on atmospheric  $\delta D$  was turned off by setting  $\delta D_{ET}$  to  $\delta D_{vapor}$  of the lowest atmospheric model level ( $S_{ET} = (\delta D \text{ from EXP2}) - (\delta D \text{ from EXP4})$ ). The strength of surface fluxes is not affected by this change.
4.  $S_{SC}$ : To assess the impact of subcloud processes, we performed the model run EXP5. Rain evaporation rates ( $E$ ) in COSMO are parametrized based on saturation humidity with respect to liquid water ( $q_{sat}$ ), specific humidity ( $q_v$ ), and a semiempirical function  $F$  of rain content ( $q_r$ ). In COSMO<sub>150</sub>, the HDO mass exchange

**Table 1**  
Model Runs and Derived Sensitivities

Name of model run	Description
EXP1	Reference run from 2010 to 2014 (section 2.1.2); horizontal wind fields above 850 hPa nudged to ECHAM-wiso “reanalysis”
EXP2	Same setup as in EXP1 but from 2000 to 2014 and without nudged wind fields
EXP3	SST decreased by 3 K; from 2000 to 2014 and without nudged wind fields
EXP4	No impact of continental evapotranspiration on $\delta D$ ; from 2000 to 2014 and without nudged wind fields
EXP5	No impact of subcloud processes on $\delta D$ ; from 2000 to 2014 and without nudged wind fields
EXP6	No impacts of continental evapotranspiration and subcloud processes on $\delta D$ ; from 2000 to 2014 and without nudged wind fields
EXP7	$\delta D$ at lateral model boundaries decreased by 10‰; from 2000 to 2014 and without nudged wind fields
Derived sensitivities	Description
$S_{TOT}$	Sensitivity of the modeled $\delta D$ to continental evapotranspiration, rainout, and subcloud processes: $(\delta D \text{ from EXP2}) - \delta D_{MBL}$ (with $\delta D_{MBL} = -90\text{‰}$ ).
$S_{SST}$	Sensitivity of the modeled $\delta D$ to a 3 K lower sea surface temperature: EXP3 – EXP2.
$S_{ET}$	Sensitivity of the modeled $\delta D$ to continental evapotranspiration: EXP2–EXP4.
$S_{SC}$	Sensitivity of the modeled $\delta D$ to subcloud processes: EXP2–EXP5.
$S_{ET+SC}$	Sensitivity of the modeled $\delta D$ to continental evapotranspiration and subcloud processes: EXP2 – EXP6.
$S_R$	Sensitivity of the modeled $\delta D$ to rainout: $S_{TOT} - S_{ET+SC} = (\delta D \text{ from EXP6}) - \delta D_{MBL}$ (with $\delta D_{MBL} = -90\text{‰}$ ).
$S_B$	Sensitivity of the modeled $\delta D$ to a changed $\delta D$ at the lateral model boundaries: EXP2–EXP7.

rate between rain drops and water vapor ( ${}^{\text{HDO}}E$ ) is calculated following Stewart (1975), who suggested a parametrization based on the isotope abundances in  $q_r$  and  $q_v$  (for details see Pfahl et al., 2012):

$${}^{\text{H}_2\text{O}}E = F({}^{\text{H}_2\text{O}}q_r) (q_{\text{sat}} - {}^{\text{H}_2\text{O}}q_v) \quad (1)$$

$${}^{\text{HDO}}E = F({}^{\text{H}_2\text{O}}q_r) \left( \frac{{}^{\text{HDO}}D}{{}^{\text{H}_2\text{O}}D} \right)^{0.58} \left( \alpha_e q_{\text{sat}} \frac{{}^{\text{HDO}}q_r}{{}^{\text{H}_2\text{O}}q_r} - {}^{\text{HDO}}q_v \right) \quad (2)$$

${}^{\text{HDO}}D$  and  ${}^{\text{H}_2\text{O}}D$  are the isotope diffusivities, and  $\alpha_e$  is the isotope fractionation factor for equilibrium conditions. The rightmost term in equation (2) depends on the gradient between isotope abundances in  $q_r$  and  $q_v$ . It forces rain and the surrounding water vapor to isotopically equilibrate and may result in significant  ${}^{\text{HDO}}E$  even in the case of a vanishing  ${}^{\text{H}_2\text{O}}E$ . For determining the impact of subcloud processes, we used the approach of (3) and suppressed the effect of subcloud processes on  $\delta D$  in the model run EXP5. We then interpret  $S_{SC} = (\delta D \text{ from EXP2}) - (\delta D \text{ from EXP5})$  as sensitivity of the modeled  $\delta D$  to subcloud processes. To this end, we set  ${}^{\text{HDO}}E = {}^{\text{H}_2\text{O}}E \cdot \frac{{}^{\text{HDO}}q_r}{{}^{\text{H}_2\text{O}}q_r}$  in EXP5. This means that  $q_r$  is still affected by rain evaporation but the  $\delta D$  of rain is not changed anymore subsequent to the formation of rain. For water vapor, this means that



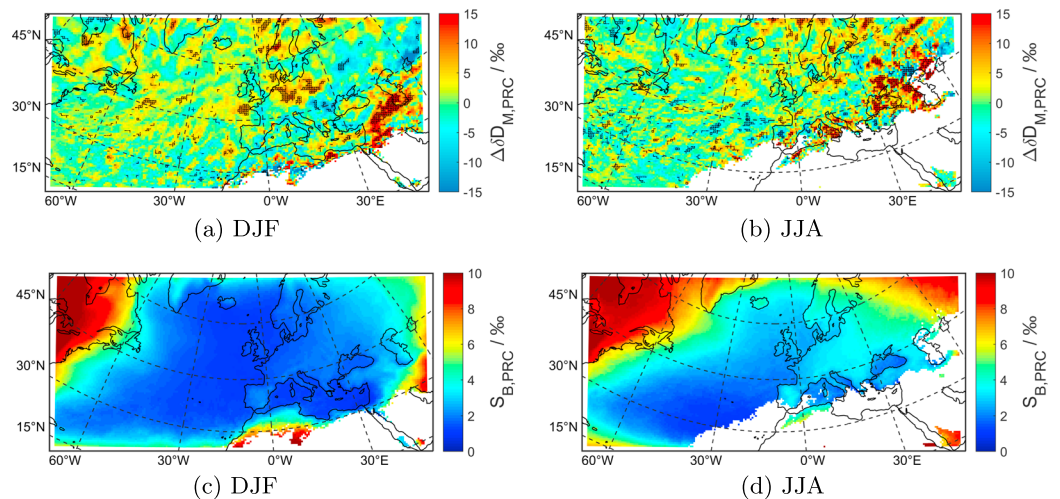


**Figure 2.** Sensitivity of the modeled  $\delta D$  in precipitation to spectral nudging and boundary data. (a and b) Mean differences between a model run with spectral nudging of wind fields (EXP1) and a model run without nudging (EXP2) for December-January-February (DJF)/June-July-August (JJA) from 1 January 2010 to 31 December 2014. Hatched areas: significant difference (mean difference greater than two standard deviations of monthly means divided by square root of number of months). (c and d) Sensitivity to a change of  $\delta D$  of water vapor at the lateral model boundaries by 10‰ ( $S_B$ ) for DJF and JJA. White pixels: modeled precipitation amount is smaller than 1 mm/month for more than 80% of the used months.

isotopic equilibration with precipitation is turned off. However, the admixture of moisture from rain evaporation still has an effect on  $\delta D_{vapor}$ . For the reason of mass conservation in the model this remaining effect on  $\delta D_{vapor}$  cannot be completely eliminated.

5.  $S_R$ : The general relation between  $\delta D$  in precipitation and temperature (Dansgaard, 1964) demonstrates the important impact of rainout on  $\delta D$  of atmospheric water. For determining the sensitivity of  $\delta D$  to rainout, we do not apply the approach of (3) and (4) because turning off the effect of rainout on  $\delta D$  would strongly change the effects of continental evapotranspiration and subcloud processes, which both depend on realistic  $\delta D$  fields. Instead, we quantified the impact of simultaneously acting continental evapotranspiration and subcloud processes on  $\delta D$  by means of the model run EXP6, in which we switched off the effects of continental evapotranspiration and subcloud processes on  $\delta D$ :  $S_{ET+SC} = (\delta D \text{ from EXP2}) - (\delta D \text{ from EXP6})$ . In EXP6 the modeled  $\delta D$  only reflects the fractionation during evaporation from the ocean and subsequent changes of  $\delta D$  due to rainout as well as a potential redistribution of  $\delta D$  values by air mass mixing. The redistribution of  $\delta D$  from air mass mixing only occurs in the case of inhomogeneous  $\delta D$  fields, which, in turn, are mainly caused by rainout. For this reason, we subsume both the direct fractionation effect during rainout and the indirect mixing effect under the term "rainout." To derive the sensitivity of  $\delta D$  to rainout, we subtracted  $S_{ET+SC}$ , which considers the impacts of continental evapotranspiration and subcloud processes on  $\delta D$ , from  $S_{TOT}$ , which considers the impacts of continental evapotranspiration, subcloud processes, and rainout on  $\delta D$ :  $S_R = S_{TOT} - S_{ET+SC}$ .
6.  $S_B$ : For quantifying the sensitivity of the modeled  $\delta D$  to  $\delta D$  provided by ECHAM-wiso at the lateral boundaries ( $S_B$ ), we shifted  $\delta D$  at the lateral model boundaries in EXP7 by  $-10\text{‰}$ .  $S_B = (\delta D \text{ from EXP2}) - (\delta D \text{ from EXP7})$  of  $\delta D$  in precipitation for December-January-February (DJF)/June-July-August (JJA) is shown in Figure 2c/2d.  $S_B$  is highest in North America, where most air masses enter the model domain. Moisture uptake from the Atlantic during the westward transport of air masses results in a rapid decrease of  $S_B$ .  $S_B$  of  $\delta D$  in central European precipitation to the 10‰ change at the boundaries is about 2‰/3‰ for DJF/JJA. The sensitivity to boundary data may result in an underestimation of the sensitivities  $S_{SST}$ ,  $S_{ET}$ ,  $S_{SC}$ , and  $S_{ET+SC}$ , which reflect the impact of specific changes only within the COSMO<sub>iso</sub> model domain. For sensitivities mainly determined by locally acting processes such as  $S_{SC}$  of  $\delta D$  in precipitation or  $S_{ET}$  of  $\delta D$  of near-surface water vapor, a respective underestimation is likely to be small. However, sensitivities, which reflect changes of large scale fields such as  $S_{SST}$ , could be underestimated by a factor of about  $(1 + \frac{S_B}{10\text{‰}})$  as changes of  $\delta D$  at the model boundaries from a globally changed SST are not considered. For this reason, we always consider the  $S_B$  when interpreting the sensitivities.

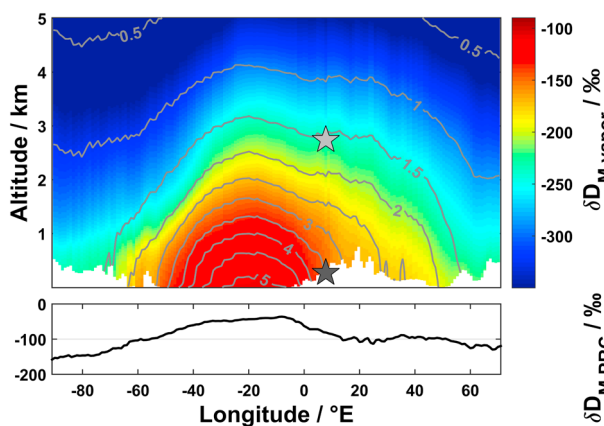


**Figure 3.** COSMO<sub>150</sub> simulation of  $\delta D_{M,vapor}$  of water vapor at 49°N in winters (December-January-February) from 2010 to 2014 (EXP1). Contour lines: humidity (g/kg); dark gray star: measurement site for the in situ observations of  $\delta D$  of near-surface water vapor and the ground-based remote sensing observations of  $\delta D$ ; light gray star: altitude level around which the ground-based remote sensing observations of  $\delta D$  is most sensitive. Lower panel: modeled  $\delta D_{M,PRC}$  in precipitation along the transect.

Table 1 gives an overview of the different model runs and of the derived sensitivities. Please note that EXP3 and  $S_{SST}$  refer to a scenario with changed climatic conditions, whereas in the other sensitivity runs only isotope fractionation differs.

## 2.2. Observations of $\delta D$

### 2.2.1. Precipitation

For comparing the COSMO<sub>150</sub> simulations with observations of  $\delta D$  in precipitation, we used data from the GNIP database. Within this network monthly accumulated precipitation samples are collected at different stations and subsequently analyzed in the laboratory with respect to their isotopic composition. The corresponding measurement uncertainty of  $\delta D$  is typically smaller than 1‰. For the simulation period from 1 January 2010 to 31 December 2014 and the used model domain of COSMO<sub>150</sub>, monthly  $\delta D$  observations from 84 GNIP stations were available. Locations of these stations are shown in Figure 1.

### 2.2.2. Ground-Based In Situ Measurements

For validating characteristics of the modeled near-surface water vapor, we used continuous measurements of specific humidity ( $q$ ) and  $\delta D$  of water vapor 28 m above the ground level (agl) in Karlsruhe in central Europe (49.10°N, 8.44°E, 110 m above sea level) from 12 January 2012 to 10 May 2013. In Figure 1 this location is indicated by the gray star.

The measurements were performed with a Picarro water isotopologue analyzer L2120-i. The observations have a temporal resolution of 0.6 Hz, a  $\delta D$  measurement accuracy smaller than 1‰, and an additional random  $\delta D$  measurement uncertainty, which for 3-hourly averages is also smaller than 1‰. Measurements of  $q$  were calibrated against observations of a nearby meteorological tower, which also provides measurements of 2 m temperature. A more detailed characterization of the Picarro isotopologue analyzer and a description of the installation and applied calibration procedures are given in Christner et al. (2017).

### 2.2.3. Ground-Based Remote Sensing Observations

In this study, we use ground-based Fourier Transform InfraRed (FTIR) observations (v2015, Type 2, Barthlott et al., 2017) of lower tropospheric  $q$  and  $\delta D$  from a NDACC station (Network for the Detection of Atmospheric Composition Change) at Karlsruhe from 17 April 2010 to 15 December 2014. For this time period, 1,756 measurements from 425 different days are available, with the duration of a single FTIR measurement being 10 min.

The remote sensing retrievals have been made in the context of the project MUSICA, for which Schneider et al. (2016) give a compact overview. From the midinfrared spectra measured by the NDACC and used for the MUSICA processing the  $\delta D$  at different altitudes can be retrieved. For the sake of simplicity, we only use retrievals of  $\delta D$  around an altitude of 2.6 km agl (Figure 4), which are well representative for the lower troposphere below 3.5 km. The remote sensing observations were empirically validated against airborne in situ measurements and therefore have a well-characterized measurement uncertainty (Schneider et al., 2016). In the lower and middle troposphere random measurement uncertainty of  $q/\delta D$  of the remote sensing observations is estimated to be  $\pm 2\%/\pm 25\%$ . The respective measurement bias of free tropospheric  $q$  and  $\delta D$  falls between  $-6$  and  $+10\%$  for  $q$  and between  $-25$  and  $+5\%$  for  $\delta D$ . The remote sensing observations are unevenly distributed in time and, being based on solar absorption spectra, limited to daytime and cloud free conditions. For comparing the remote sensing observations with the 3-hourly model output of COSMO<sub>150</sub>, we excluded model data without an observation within  $\pm 1.5$  h. In the case that there was more than one observation within  $\pm 1.5$  h, we only used the observation closest in time to the model output. To account for the sensitivity of the remote sensing observations to  $\delta D$  at different altitudes, we applied the averaging kernels of the remote sensing observations also to the model data. A typical averaging kernel is shown in Figure 4, indicating that values retrieved for 2.6 km mainly reflect the atmospheric  $q$  and  $\delta D$  state in the lower troposphere between a few hundred meters

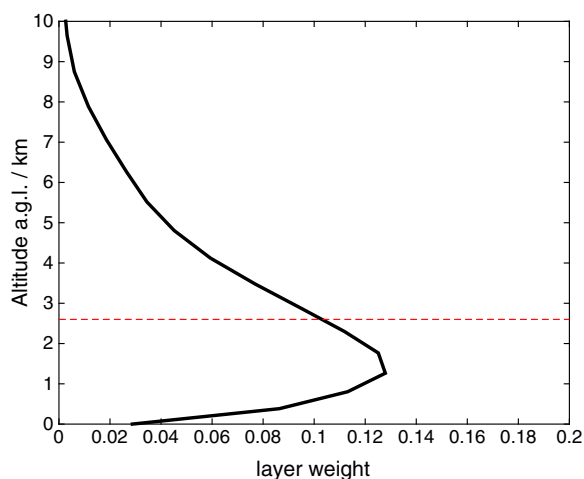


**Figure 4.** Typical logarithmic averaging kernel for the  $\delta D$  proxy state 2.6 km above ground level as retrieved from the ground-based Network for the Detection of Atmospheric Composition Change/FTIR spectra in Karlsruhe. The graph displays the altitude regions that mainly contribute to the retrieved  $\delta D$ . Red line: Kernel-weighted altitude.

above ground level and about 3.5 km agl. The matrix elements  $\partial \ln \hat{x} / \partial \ln x$  of the averaging kernel matrix  $\mathbf{A}$  characterize the retrieval product and quantify changes of the retrieved concentration  $\hat{x}$  for changes of the actual atmospheric concentration  $x$  according to

$$(\ln \hat{\mathbf{x}} - \ln \mathbf{x}_a) = \mathbf{A}(\ln \mathbf{x} - \ln \mathbf{x}_a), \quad (3)$$

whereby  $\mathbf{x}_a$  is the a priori concentration profile, which a retrieval is constrained to, and  $\hat{\mathbf{x}}$ ,  $\mathbf{x}$ , and  $\mathbf{x}_a$  are vectors with  $3 \times 28$  entries denoting the retrieved, the actual, and the a priori concentrations of  $\text{H}_2^{16}\text{O}$ ,  $\text{HD}^{16}\text{O}$ , and  $\text{H}_2^{18}\text{O}$  at 28 altitude levels between 0 and 55 km (for a detailed description of the MUSICA NDACC/FTIR data products and recipes ensuring their correct application please see Barthlott et al., 2017). Note that also  $\text{H}_2^{18}\text{O}$  is retrieved to account for cross dependency of retrieved concentrations of  $\text{H}_2^{16}\text{O}$  and  $\text{HD}^{16}\text{O}$  on  $\text{H}_2^{18}\text{O}$ . For applying  $\mathbf{A}$  to the modeled concentrations ( $\mathbf{m}$ ) of  $\text{H}_2^{16}\text{O}$ ,  $\text{HD}^{16}\text{O}$ , and  $\text{H}_2^{18}\text{O}$ , we first linearly interpolated the model state vector  $\mathbf{m}$  to the altitude level scheme used for the state vector (and  $\mathbf{A}$ ). For altitudes above the model top layer at 21.5 km, we used the isotope concentrations of  $\mathbf{x}_a$  also for  $\mathbf{m}$ . We then derived the vertically smoothed  $\hat{\mathbf{m}}$  according to

$$\hat{\mathbf{m}} = \exp[\mathbf{A}(\ln \mathbf{m} - \ln \mathbf{x}_a) + \ln \mathbf{x}_a]. \quad (4)$$

The entries of  $\hat{\mathbf{m}}$  can be directly compared with the entries of  $\hat{\mathbf{x}}$ .

### 3. Comparison of COSMO<sub>iso</sub> Simulations With Multiplatform $\delta\text{D}$ Observations

Figure 3 shows the modeled winter mean  $\delta\text{D}$  of water vapor over Europe (2010–2014) along a longitudinal cross section at  $49^\circ\text{N}$ . The well-known rainout-induced climatological vertical and continental gradients in  $\delta\text{D}$  are clearly visible in the figure.  $\delta\text{D}$  is highest in the freshly evaporated water vapor in the marine boundary layer and decreases with altitude by about  $50\text{‰}/\text{km}$  as expected from the colder temperature and the high degree of rainout. A clear longitudinal gradient of  $\delta\text{D}$  is visible over Europe, reflecting the increasing degree of rainout of air masses over the continent with distance to the coast. Because  $\delta\text{D}$  in precipitation depends on the  $\delta\text{D}$  of the water vapor which it is formed from, also the modeled  $\delta\text{D}$  in precipitation ( $\delta\text{D}_{\text{M,PRC}}$ ) shows this well-known continental effect (lower panel in Figure 3). In addition to the continental effect, the latitude effect and the altitude effect are illustrated (Figure 5a) by the latitudinal gradient of  $\delta\text{D}_{\text{M,PRC}}$  and the relatively low modeled  $\delta\text{D}_{\text{M,PRC}}$  values in mountainous regions such as the Alps ( $47^\circ\text{N}$ ,  $10^\circ\text{E}$ ).

In this section, we compare the COSMO<sub>iso</sub> simulations with observations to quantitatively evaluate the modeled  $\delta\text{D}$ . To this end, we first validate  $\delta\text{D}_{\text{M,PRC}}$  in European precipitation. Subsequent to this, we validate  $\delta\text{D}$  in central Europe, based on data from a station with simultaneous observations of  $\delta\text{D}$  in precipitation,  $\delta\text{D}$  of water vapor around 2.6 km agl, and  $\delta\text{D}$  in continental near-surface water vapor. Figures 1 and 3 show the respective sampling locations.

#### 3.1. $\delta\text{D}$ in Precipitation

Figures 5a and 5b show model-data comparisons for European  $\delta\text{D}_{\text{PRC}}$  during winters (DJF) and summers (JJA) from 2010 to 2014. In the following, we use the subscripts O and M to indicate if a variable refers to observations or model output, respectively. For both seasons, the modeled  $\delta\text{D}_{\text{M,PRC}}$  shows the continental effect, the latitude effect, and the altitude effect, with the continental  $\delta\text{D}_{\text{M,PRC}}$  being generally lowest in DJF. These characteristics are in good agreement with the observed  $\delta\text{D}_{\text{O,PRC}}$  at GNIP stations. In particular in winter, the agreement with continental as well as with most coastal GNIP stations is good. In summer, the agreement is best for western Europe, whereas  $\delta\text{D}_{\text{M,PRC}}$  east of  $5^\circ\text{E}$  tends to show moderate high biases of about 10 to 20‰.

Figure 5c shows the comparison between the monthly  $\delta\text{D}_{\text{M,PRC}}$  and  $\delta\text{D}_{\text{O,PRC}}$  from all European GNIP stations with data available between 2010 and 2014. The color code in Figure 5c depicts the modeled air temperatures 2 m agl ( $T_{\text{M,2m}}$ ) at the respective GNIP stations and again illustrates the close relation between air temperature and  $\delta\text{D}$ . Note that monthly air temperature in central Europe is closely related to season. For this reason, reproducing the temperature dependence of  $\delta\text{D}$  in the model means reproducing the seasonality of  $\delta\text{D}$ , and vice versa. A high squared correlation coefficient ( $R^2$ ) of 0.67 demonstrates that COSMO<sub>iso</sub> is not only able to capture the climatological seasonal characteristics of  $\delta\text{D}_{\text{O,PRC}}$  (Figure 5a/5b) but also the monthly  $\delta\text{D}_{\text{O,PRC}}$  during individual months and years. The average difference between monthly  $\delta\text{D}_{\text{M,PRC}}$  and  $\delta\text{D}_{\text{O,PRC}}$  is  $+3\text{‰}$  with a standard deviation of differences between  $\delta\text{D}_{\text{M,PRC}}$  and  $\delta\text{D}_{\text{O,PRC}}$  of 19‰. Measurement uncertainty related to the analysis of  $\delta\text{D}$  in precipitation samples is smaller than  $\pm 1\text{‰}$  and can only explain a small part of the scatter. More important sources of uncertainty may be sampling errors and limited spatial representativeness



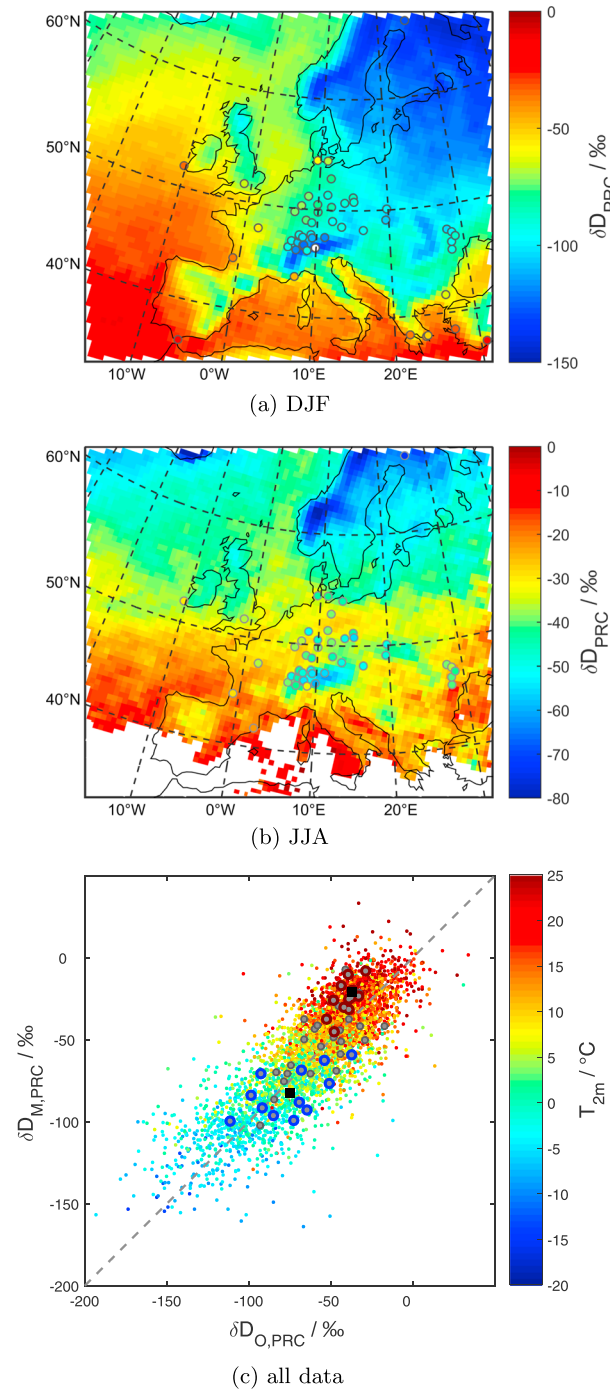


**Figure 5.**  $\delta D$  in European precipitation from 2010 to 2014. (a) Model-data comparison with Global Network of Isotopes in Precipitation (GNIP) data for December-January-February (DJF). Colored area: mean modeled  $\delta D$  in precipitation; colored dots: GNIP observations (only stations with data from at least 10 winter months are included in this figure to assure representativeness for the modeled time period). (b) Same as (a) but for June-July-August (JJA) and on a different color scale. White pixels: modeled precipitation amount is smaller than 1 mm/month for more than 80% of the used months. (c) Model-data comparison with all European GNIP observations from 2010 to 2014 ( $R^2 = 0.67$ ). Each dot represents  $\delta D$  at one GNIP station from a single month. Color:  $T_{M,2m}$  at the corresponding GNIP station; gray dashed line: 1:1; gray dots: data from Karlsruhe (blue edge: DJF and red edge: JJA); black squares: means for Karlsruhe for DJF/JJA.

of GNIP stations, in particular in mountainous regions. Another important part of the scatter between  $\delta D_{M,PRC}$  and  $\delta D_{O,PRC}$  is likely to be caused by uncertainty of the modeled  $\delta D_{M,PRC}$ . Note that this model uncertainty may result from both model physics and errors in the representation of the meteorological situation due to the imperfect nudging scheme. In addition to the scatter between  $\delta D_{M,PRC}$  and  $\delta D_{O,PRC}$ , we find a high bias of  $+8 \pm 1\%$  for  $\delta D_{M,PRC}$  during JJA. The  $\delta D_{M,PRC}$  during DJF differs from the observations by only  $-4 \pm 1\%$ . In the following, we will refer to respective data from JJA and DJF by adding "JJA" or "DJF" to the index of a variable. For Karlsruhe (49.10°N, 8.44°E) in central Europe the model bias of  $\delta D_{M,PRC,JJA}/\delta D_{M,PRC,DJF}$  is in the same order of magnitude ( $+16 \pm 2\%$ / $-8 \pm 5\%$ ) as for the other GNIP stations. The reasons for these seasonally different  $\delta D_{M,PRC}$  biases will be discussed in more detail in section 4.4.

### 3.2. $\delta D$ of Water Vapor in the Free Troposphere

Prerequisite for reliable simulations of  $\delta D$  is a reliable representation of atmospheric dynamics, temperature, precipitation amount, and specific humidity ( $q$ ) in the model. For consistently validating the modeled  $q$  and  $\delta D$  of free tropospheric water vapor, we used ground-based remote sensing observations of  $q$  ( $q_{O,FT}$ ) and  $\delta D$  ( $\delta D_{O,FT}$ ). For comparing  $q_{O,FT}$  and  $\delta D_{O,FT}$  with the model, we applied the averaging kernel of the remote sensing observations (Figure 4) to the modeled  $q_{M,FT}$  and  $\delta D_{M,FT}$  (see section 2.2.3).

Figure 6a compares the COSMO<sub>iso</sub> simulation with  $q_{O,FT}$  on a 3-hourly time scale. The  $R^2$  between  $\log(q_{O,FT})$  and  $\log(q_{M,FT})$  is  $R^2 = 0.82$  (0.75 on nonlogarithmic scale), demonstrating that COSMO<sub>iso</sub> is able to capture most of the variations of  $q_{O,FT}$ . The still existing moderate scatter between  $q_{O,FT}$  and  $q_{M,FT}$  can mainly be attributed to uncertainty of the model as the random observational error of  $q_{O,FT}$  is only 2%. Like for  $\delta D_{M,PRC}$ , this model uncertainty may result from model physics and/or the meteorology. More specifically, uncertainties in  $q_{M,FT}$  and  $\delta D_{M,FT}$  may result from errors in the representation of the boundary layer height. In addition to the scatter,  $q_{M,FT}$  is on average 8% lower than  $q_{O,FT}$ , which could be the consequence of a potential low bias of  $q_{M,FT}$  or of a potential observational high bias (Schneider et al., 2016, document the possibility of a bias between  $-6$  and  $+10\%$ ).

The  $\delta D_{O,FT}$  is reproduced by COSMO<sub>iso</sub> with a  $R^2 = 0.73$  (Figure 6b). The standard deviation of differences between  $\delta D_{M,FT}$  and  $\delta D_{O,FT}$  is 27%. Considering the uncertainty of  $q_{M,FT}$  discussed above, it is likely that part of the scatter between  $\delta D_{M,FT}$  and  $\delta D_{O,FT}$  is caused by model uncertainty. The other part of the scatter is a consequence of a random error of  $\delta D_{O,FT}$  of about  $\pm 25\%$ . For determining the mean deviation between  $\delta D_{M,FT}$  and  $\delta D_{O,FT}$ , we used weekly binned differences between  $\delta D_{M,FT}$  and  $\delta D_{O,FT}$  to account for an especially high sample density during certain time periods. For this purpose, the time period of observations was split into 244 consecutive weekly bins, covering the  $\delta D_{O,FT}$  from 17 April 2010 to 15 December 2014. The mean of the binned differences between  $\delta D_{M,FT}$  and  $\delta D_{O,FT}$  is  $+30 \pm 2\%$  ( $\pm$  states the statistical uncertainty of the mean difference). A high bias of  $\delta D_{M,FT}$  would be in line with high biases of midtropospheric  $\delta D$  also suspected for other models (Risi et al., 2012b; Werner et al., 2011) and could be caused by different model-related issues, which are shortly discussed subsequently. Midtropospheric  $\delta D$  is especially sensitive to an overestimation of diffusive or convective vertical transport in models (Field et al., 2014; Risi et al., 2012b). Such an overestimation would increase the contribution of moisture from surface evaporation with relatively high  $\delta D$  to free tropospheric water vapor. Furthermore, an overestimation of vertical transport might strengthen mixing of dry and moist air masses, which decouples  $\delta D$  and specific humidity from a relation expected for rainout and generally increases the average  $\delta D$ . In addition, a high bias of  $\delta D$  at the lateral model boundaries, which for ECHAM5-wiso could be on the order of 30% (Schneider et al., 2017; Werner et al., 2011), would result in a bias of  $\delta D_{M,FT}$  of about  $\frac{S_B}{10\%} \cdot 30\% = 0.29 \cdot 30\% = +9\%$  (for  $S_B$  of water vapor in Karlsruhe at 2.6 km agl of 2.9%). On the other hand, the difference between  $\delta D_{M,FT}$  and  $\delta D_{O,FT}$  may also partly be caused by a potential low bias of the remote sensing observations (between  $-25$  and  $+5\%$ , according to Schneider et al., 2016) or may even be completely explained by a bias of the observations if considering the confidence range of the observational bias. The last interpretation is supported by the comparison between  $q_{O,FT}$  and  $q_{M,FT}$ , since, because of the generally positive relation between  $\delta D$  and  $q$ , it is unlikely to find a low bias of  $q_{M,FT}$  and a high bias of  $\delta D_{M,FT}$  in the model. However, a clear attribution of the differences between  $\delta D_{M,FT}$  and  $\delta D_{O,FT}$  to a bias of the model or the observations is not possible from this comparison. The differences between  $\delta D_{M,FT}$  and  $\delta D_{O,FT}$  are similar for JJA and DJF:  $+24 \pm 2\%$  and  $+35 \pm 6\%$ , respectively. Therefore, the main conclusions from the model-data comparison with remote sensing observations are that the model realistically represents the variations of  $\delta D$  in the lower free troposphere (good correlation) and that a potential high bias of  $\delta D_{M,FT}$  does not strongly depend on temperature (similar differences for DJF and JJA).

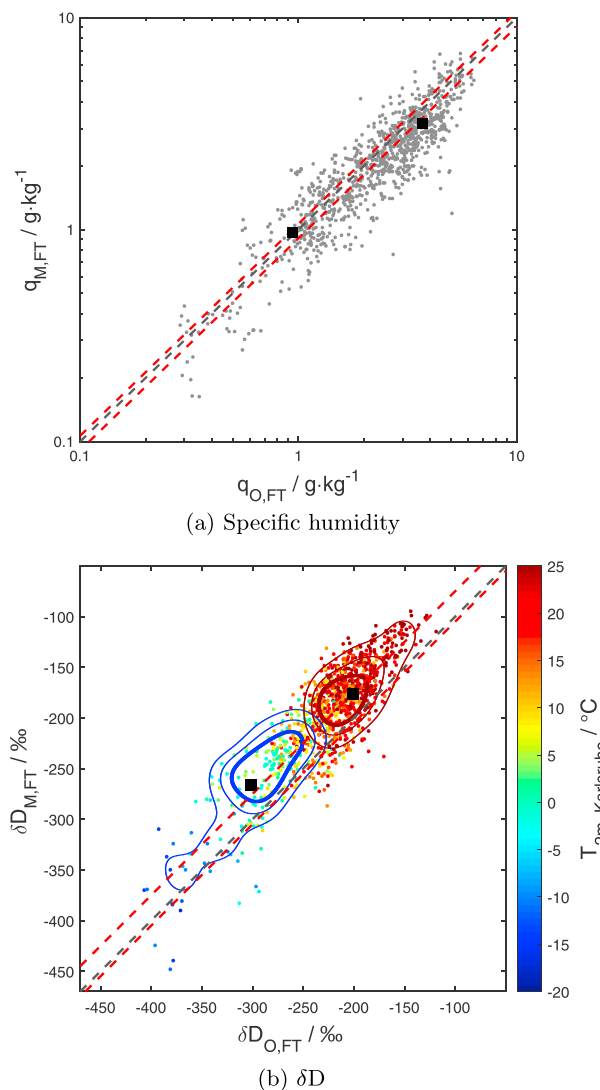


**Figure 6.** Specific humidity ( $q$ ) and  $\delta D$  of water vapor around 2.6 km above ground level in Karlsruhe from 2010 to 2014. Each dot represents one observation and the model output closest in time to the observation. Gray dashed lines: 1:1; red dashed lines: possible model-data difference due to a potential observational bias according to Schneider et al. (2016); black squares: averages for December-January-February and June-July-August, based on weekly binned differences between  $q_{M,FT}$  and  $q_{O,FT}$  or  $\delta D_{M,FT}$  and  $\delta D_{O,FT}$ . (a) Model-data comparison with ground-based remote sensing observations of  $q$  ( $R^2 = 0.82$ ). (b) Same as in (a) but for  $\delta D$  ( $R^2 = 0.73$ ). Contour lines: two-dimensional probability distributions of the modeled and observed  $\delta D$  from December-January-February (blue)/June-July-August (red). The different contour lines indicate probabilities of occurrence of 0.7, 0.5, and 0.3 (normalized to 1 at the maximum).

### 3.3. $\delta D$ of Near-Surface Water Vapor

Specific humidity and near-surface temperature determine relative humidity at the ground level. Thereby, they exert a major control on evaporation rates as well as on the strength of isotope fractionation during surface evaporation. For evaluating the modeled  $\delta D$  of near-surface water vapor, we also validated the modeled  $T_{M,2m}$  in addition to specific humidity. Figure 7 shows the model-data comparisons for  $T_{M,2m}$ ,  $q_{M,SFC}$ , and  $\delta D_{M,SFC}$  of near-surface water vapor with in situ measurements in Karlsruhe ( $T_{O,2m}$ ,  $q_{O,SFC}$ , and  $\delta D_{O,SFC}$ ). To account for the different temporal resolution of the 3-hourly model output and the much higher time resolution of  $T_{O,2m}$ ,  $q_{O,SFC}$ , and  $\delta D_{O,SFC}$ , we calculated 3-hourly arithmetic means from the measurements.

Figure 7a compares the modeled and observed  $T_{2m}$  in Karlsruhe ( $R^2 = 0.92$ ) and illustrates the correspondence between season and temperature. For summer, we find a small model bias of  $T_{M,2m,JJA}$  in Karlsruhe of  $-0.4$  K. In winter,  $T_{M,2m,DJF}$  has a slightly larger bias of  $-2.0$  K. Consistent with the realistic  $T_{M,2m}$ , the modeled

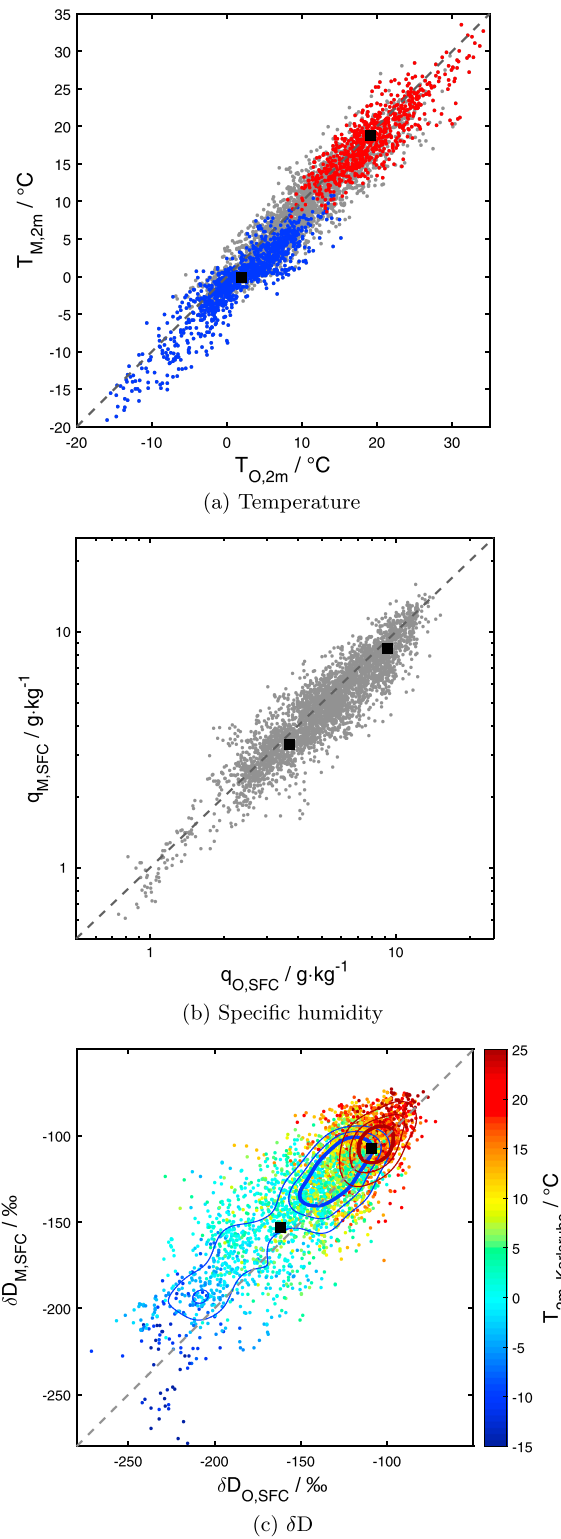


**Figure 7.**  $T_{2m}$ , specific humidity, and  $\delta D$  of near-surface water vapor in Karlsruhe from January 2012 to May 2013. Each dot represents a 3 h average of observations and the respective model output. Gray dashed lines: 1:1; black squares: mean deviation between model and observation for December-January-February (DJF)/June-July-August (JJA). (a) Model-data comparison for  $T_{2m}$  ( $R^2 = 0.92$ ). The blue/red color indicates data from DJF/JJA. (b) Model-data comparison for specific humidity ( $R^2 = 0.85$ ). (c) Model-data comparison for  $\delta D$  ( $R^2 = 0.69$ ). Color:  $T_{M,2m}$  in Karlsruhe; contour lines: two-dimensional probability distributions of the modeled and observed  $\delta D$  from DJF (blue)/JJA (red). The different contour lines indicate probabilities of occurrence of 0.7, 0.5, and 0.3 (normalized to 1 at the maximum).

$q_{M,SFC}$  also is in good agreement with the observed  $q_{O,SFC}$  (Figure 7b). We find a  $R^2 = 0.85$  between  $\log(q_{M,SFC})$  and  $\log(q_{O,SFC})$  (0.83 on nonlogarithmic scale) and a small bias of  $q_{M,SFC}$  of  $-4\%$ .

Figure 7c shows the comparison of  $\delta D_{M,SFC}$  and  $\delta D_{O,SFC}$ . Considering a measurement uncertainty of  $\delta D_{O,SFC}$  smaller than  $\pm 1\%$ , the standard deviation of differences between  $\delta D_{M,SFC}$  and  $\delta D_{O,SFC}$  of  $20\%$  can mainly be attributed to uncertainty of the model. For summer, the  $\delta D_{M,SFC,JJA}$  values are on average  $+2 \pm 1\%$  higher than  $\delta D_{O,SFC,JJA}$ . The  $\delta D_{M,SFC,DJF}$  values are biased by  $+8 \pm 1\%$ . In comparison to the values of  $\delta D_{M,SFC}$ , the biases are relatively small, implying a realistic implementation of the most important processes controlling the  $\delta D_{M,SFC}$  in Karlsruhe. In spite of the higher quality of observations, the scatter is slightly larger for near-surface compared to free atmospheric data, which may be due to local effects such as surface heterogeneity, which would need higher horizontal grid resolution to be correctly represented.

### 3.4. Summary of Comparisons

COSMO<sub>iso</sub> is capable of realistically reproducing most of the spatial and seasonal characteristics of  $\delta D_{O,PRC}$  as well as the variations of  $\delta D$  that were captured by the different multiplatform observations. We found the model biases of  $\delta D_{M,FT}$ ,  $\delta D_{M,SFC}$ , and  $\delta D_{M,PRC}$  to be mostly positive but relatively small in comparison to the absolute  $\delta D$  values of water vapor or precipitation. In addition, the biases were almost independent of temperature. Together, these findings imply a reliable representation and interplay of the most important isotope fractionation processes in COSMO<sub>iso</sub> and justify the application of this model for characterizing the impacts of different isotope effects, which are presented in the next section.

## 4. Sensitivities to Different Processes

In this section, we employ COSMO<sub>iso</sub> to characterize impacts of the most important fractionation processes controlling the  $\delta D$  of atmospheric water in Europe. To this end, we first analyze the sensitivities of the European  $\delta D_{M,PRC}$  to conditions at the ocean surface and different isotope fractionation processes. In a second step, the sensitivity study is complemented by sensitivity estimates of  $\delta D_{M,FT}$  and  $\delta D_{M,SFC}$  in Karlsruhe (central Europe).

### 4.1. Sensitivities of European $\delta D_{M,PRC}$

Figure 8 shows the sensitivities of  $\delta D_{M,PRC}$  to the total isotope fractionation impacting atmospheric water ( $S_{TOT}$ ), rainout ( $S_R$ ), continental evapotranspiration ( $S_{ET}$ ), subcloud processes ( $S_{SC}$ ), and conditions over the ocean ( $S_{SST}$ ). For identifying the seasonality of sensitivities, the figure distinguishes sensitivities for winter and summer. A detailed definition of the sensitivities is given in section 2.1.3.

$S_{TOT}$  gives the total impact of isotope fractionation processes relative to the mean isotopic composition of water vapor in the marine boundary layer ( $\delta D_{MBL} = -90\%$ ). So  $S_{TOT}$  of  $\delta D_{M,PRC}$  (Figure 8a/8b) shows the same spatial patterns as  $\delta D_{M,PRC}$  (Figure 5a/5b), with  $S_{TOT}$  being  $90\%$  higher than  $\delta D_{M,PRC}$ . This results in positive  $S_{TOT}$  in warm marine regions, where  $\delta D_{M,PRC}$  is less negative than  $\delta D_{MBL}$ . Like  $\delta D_{M,PRC}$ ,  $S_{TOT}$  of  $\delta D_{M,PRC}$  is strongly temperature dependent and shows most negative values in winter.

The response of European  $\delta D$  in precipitation to slightly changed conditions at the marine moisture sources is small as illustrated by the small  $S_{SST}$  of  $\delta D_{M,PRC}$  for a 3 K change of SST (Figure 8c/8f). In winter,  $S_{SST,DJF}$  of European  $\delta D_{M,PRC}$  is on the order of  $-10\%$ .  $S_{SST,JJA}$  of  $\delta D_{M,PRC}$  is close to 0.

$S_{TOT,DJF}$  (Figure 8a) and  $S_{R,DJF}$  (Figure 8d) of European  $\delta D_{M,PRC,DJF}$  show similar spatial patterns, with longitudinal gradients being larger for  $S_{TOT,DJF}$ . Because the impact of continental evapotranspiration on  $\delta D_{M,PRC,DJF}$  ( $S_{ET,DJF}$ , Figure 8g) is small, subcloud processes ( $S_{SC,DJF}$ , Figure 8i) are the major driver of this difference between  $S_{TOT,DJF}$  and  $S_{R,DJF}$ . In marine regions, the interaction of precipitation with relatively enriched surface vapor causes an enrichment of the precipitation and a depletion of the remaining vapor. This leads to positive values of  $S_{SC,DJF}$  over the ocean. However, due to the inland transport of the more depleted vapor, which serves as the moisture source for precipitation further downstream,  $S_{SC,DJF}$  changes sign over the continents (see also Field et al., 2010).

In summer,  $S_{TOT,JJA}$  (Figure 8b) of  $\delta D_{M,PRC}$  is more positive than in winter. Despite warmer temperatures and higher specific humidity in summer,  $S_{R,JJA}$  (Figure 8e) of central European  $\delta D_{M,PRC}$  is very similar to  $S_{R,DJF}$  in winter (Figure 8d). This implies similar degrees of rainout of European lower tropospheric air masses in summer and in winter. The most important reason for the higher  $S_{TOT,JJA}$  in summer is the enhanced impact of continental evapotranspiration ( $S_{ET,JJA}$ , Figure 8h). This effect almost overcompensates the continental gradient of  $S_{R,JJA}$ . A second important reason is the impact of subcloud processes ( $S_{SC,JJA}$ , Figure 8j), which further



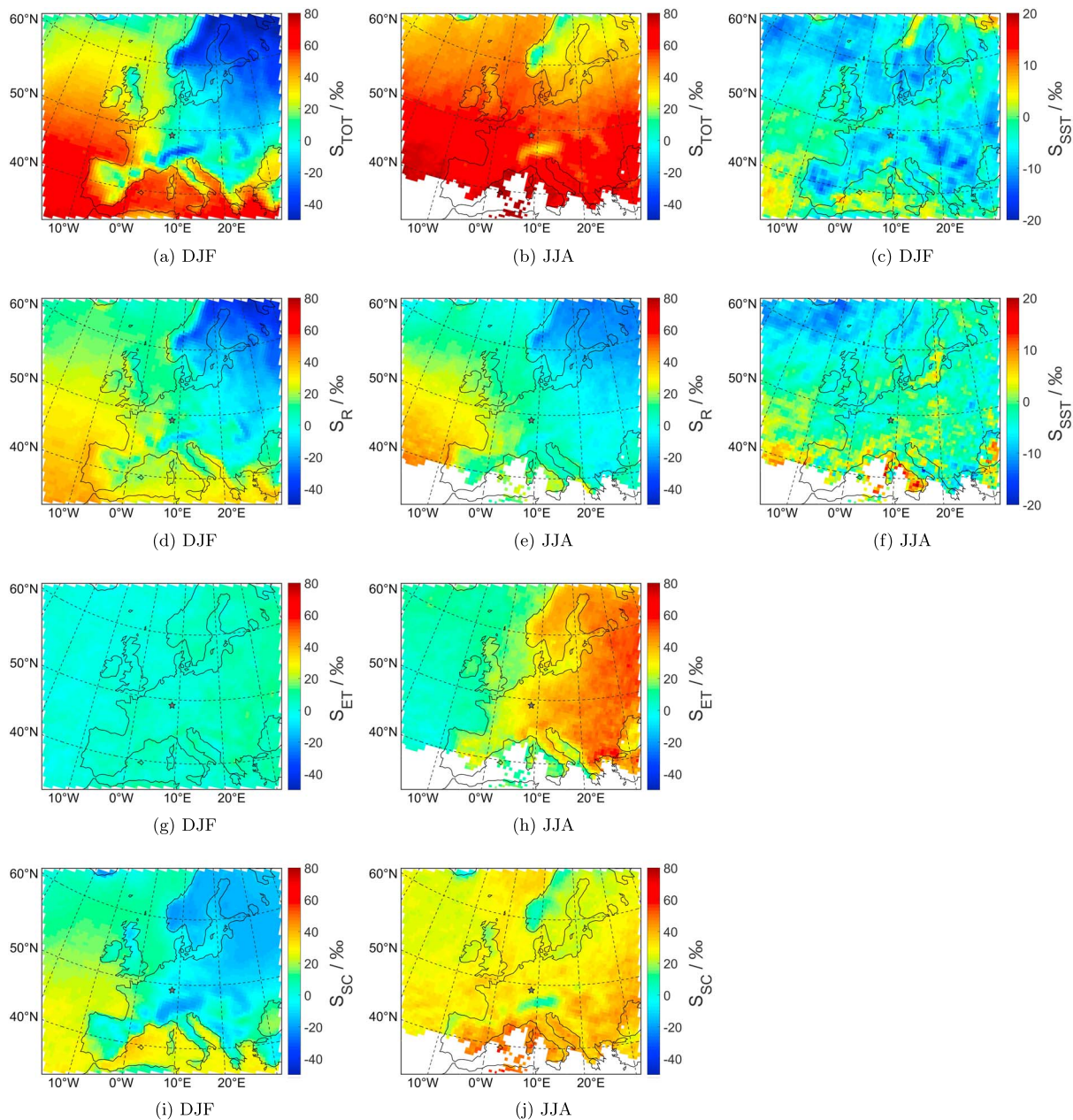
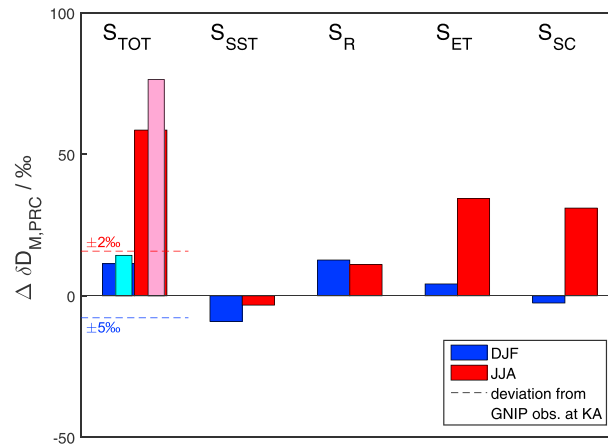


**Figure 8.** Sensitivities of the modeled  $\delta D$  in European precipitation to the total isotope fractionation acting on atmospheric water (a and b:  $S_{TOT}$ ), rainout (d and e:  $S_R$ ), continental evapotranspiration (g and h:  $S_{ET}$ ), subcloud processes (i and j:  $S_{SC}$ ), and conditions over the ocean (c and f:  $S_{SST}$ ) for December-January-February (DJF)/June-July-August (JJA) from 2000 to 2014. Gray star: multiplatform observations at Karlsruhe. Note that  $S_{SST}$  is shown on a different scale. White pixels: modeled precipitation amount is smaller than 1 mm/month for more than 80% of the used months.

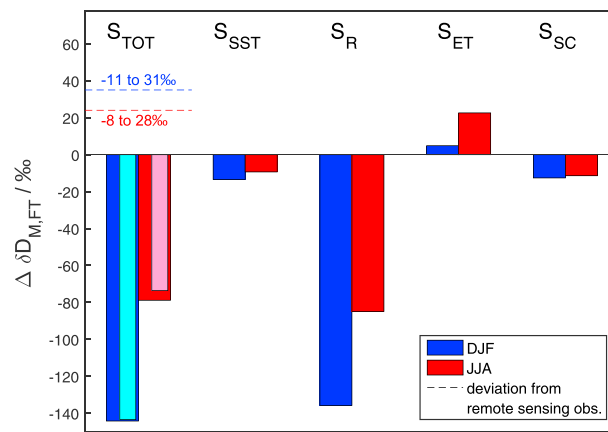
increases  $\delta D_{M,PRC,JJA}$ . The last finding is in line with sensitivity experiments by Field et al. (2010), who find post condensation isotope exchange in Europe during summer to systematically enrich heavy isotopes in precipitation, and a case study by Aemisegger et al. (2015), who investigated the role of subcloud processes during a cold front passage in Zurich, Switzerland. In particular under warmer conditions, the European  $\delta D$  is therefore far from being a pure rainout signal.

#### 4.2. Sensitivities of $\delta D_{M,FT}$ and $\delta D_{M,SFC}$ in Central Europe

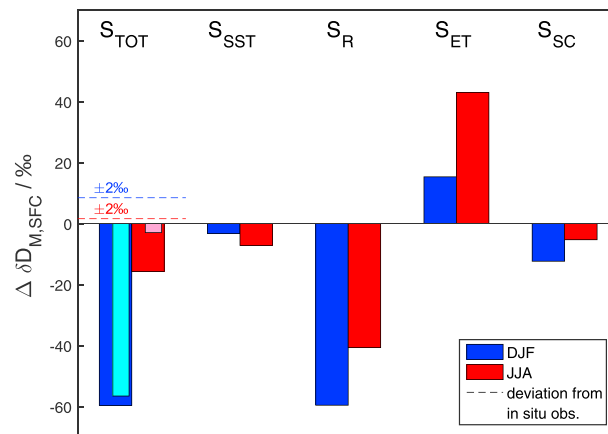
For investigating sensitivities of  $\delta D$  of water vapor, we use model results for Karlsruhe. For this location realistic model values of lower tropospheric water vapor ( $\delta D_{M,FT}$ ) and continental near-surface water vapor ( $\delta D_{M,SFC}$ ) are confirmed by the model-data comparisons in section 3. Figure 9 shows the respective sensitivities



(a)  $\delta D$  in precipitation



(b)  $\delta D$  of free tropospheric water vapor



(c)  $\delta D$  of near-surface water vapor

**Figure 9.** Sensitivities of  $\delta D_{M,PRC}$ ,  $\delta D_{M,FT}$ , and  $\delta D_{M,SFC}$  in Karlsruhe: impacts of the total isotope fractionation acting on atmospheric water ( $S_{TOT}$ ), conditions over the ocean ( $S_{SST}$ ), rainout ( $S_R$ ), continental evapotranspiration ( $S_{ET}$ ), and subcloud processes ( $S_{SC}$ ) on the modeled  $\delta D$  in Karlsruhe for December-January-February (DJF) (blue)/June-July-August (JJA) (red) from 2000 to 2014. Thin light blue and light red bars depict the sums of  $S_R$ ,  $S_{ET}$ , and  $S_{SC}$ . Dashed lines: mean deviation between the modeled and observed  $\delta D$  in Karlsruhe; attached numbers give the sum of statistical uncertainty of a model-data comparison and the possible model-data difference caused by a potential observational bias. (a) Impacts on  $\delta D_{M,PRC}$ . The sensitivity of  $\delta D_{M,PRC}$  to a 10‰ change of  $\delta D$  at the lateral model boundaries was  $S_{B,DJF} = 1.6\text{‰}/S_{B,JJA} = 3.1\text{‰}$ . (b) Impacts on  $\delta D_{M,FT}$  ( $S_{B,DJF} = 2.4\text{‰}/S_{B,JJA} = 3.8\text{‰}$ ). (c) Impacts on  $\delta D_{M,SFC}$  ( $S_{B,DJF} = 1.4\text{‰}/S_{B,JJA} = 2.8\text{‰}$ ). GNIP = Global Network of Isotopes in Precipitation.

for winter (blue bars) and summer (red). For convenience, also sensitivities for  $\delta D_{M,PRC}$  at Karlsruhe (Figure 9a) are depicted, which are the same as the values marked by a gray star in the sensitivity maps (Figure 8).

As for  $\delta D_{M,PRC}$ ,  $S_{TOT,DJF}$  of  $\delta D_{M,FT}$  (Figure 9b) and  $\delta D_{M,SFC}$  (Figure 9c) in winter is more negative than  $S_{TOT,JJA}$  for summer. The most important difference between  $S_{TOT}$  of precipitation and water vapor is the positive value of  $S_{TOT}$  of  $\delta D_{M,PRC}$ , which is a consequence of the additional fractionation during precipitation formation.

Consistent with  $S_{SST}$  of  $\delta D_{M,PRC}$ ,  $S_{SST}$  of  $\delta D_{M,FT}$  and  $\delta D_{M,SFC}$  has negative values. However, the seasonality of  $S_{SST}$  is different for  $\delta D_{M,PRC}$ ,  $\delta D_{M,FT}$ , and  $\delta D_{M,SFC}$ . Both the seasonality of  $S_{SST}$  and the opposing seasonal response of  $S_{SST}$  found for  $\delta D_{M,PRC}$ ,  $\delta D_{M,FT}$ , and  $\delta D_{M,SFC}$  imply a nonlinear dependence of  $\delta D$  on ocean temperature and underpin a complex interplay between different fractionation processes.

In winter, the magnitudes of  $S_{TOT,DJF}$  and  $S_{R,DJF}$  are similar for  $\delta D_{M,PRC}$ ,  $\delta D_{M,FT}$ , and  $\delta D_{M,SFC}$ . This identifies rainout as the most important fractionation process determining  $\delta D$  in central Europe in winter. Superimposed to this rainout effect is the effect of continental evapotranspiration ( $S_{ET}$ ).  $\delta D$  of near-surface water vapor shows the highest  $S_{ET}$  (Figure 9c): For  $\delta D_{M,SFC,DJF}$ ,  $S_{ET,DJF}$  is about 15‰, which is 26% of the respective value of  $S_{TOT,DJF}$ . For  $\delta D_{M,PRC,DJF}$  and  $\delta D_{M,FT,DJF}$  (Figure 9a/b),  $S_{ET,DJF}$  is relatively small, implying a small contribution of continental evapotranspiration to the moisture at higher altitudes and at the condensation level.

In summer,  $S_{TOT,JJA}$  of  $\delta D_{M,FT,JJA}$ ,  $\delta D_{M,SFC,JJA}$ , and  $\delta D_{M,PRC,JJA}$  in Karlsruhe is less negative than in winter. One important reason for the higher  $S_{TOT,JJA}$  in summer is the enhanced impact of continental evapotranspiration. A second reason, which is only important for  $S_{TOT}$  of water vapor (Figure 9b/9c) are less negative values of  $S_{R,JJA}$ . For  $\delta D_{M,PRC}$  in Karlsruhe,  $S_{R,JJA}$  and  $S_{R,DJF}$  are similar (Figure 9a). An explanation for this different characteristic of  $S_R$  of  $\delta D_{M,PRC}$  compared to  $S_R$  of  $\delta D_{M,FT}$  and  $\delta D_{M,SFC}$  could be a link between rainy conditions and relatively cold air masses with  $\delta D$  of water vapor being lower than the seasonal average in summer and relatively warm and moist air masses with  $\delta D$  of water vapor being higher than the seasonal average in winter. A third reason for the differences between  $S_{TOT,JJA}$  and  $S_{TOT,DJF}$ , which is most relevant for precipitation and not so strong for water vapor, is the enhanced impact of subcloud processes on  $\delta D$ : At Karlsruhe,  $S_{SC,JJA}$  of  $\delta D_{M,PRC}$  accounts for 53% of the  $S_{TOT,JJA}$  of  $\delta D_{M,PRC}$ .

### 4.3. Feedback Between Processes

Based on the different sensitivity runs, it is possible to quantify the feedback between different fractionation processes in the model. To this end, we summed up  $S_R$ ,  $S_{ET}$ , and  $S_{SC}$  (thin light blue and light red bars in Figure 9). We refer to these sums as  $S_{TOT,SUM}$ . In winter,  $S_{TOT,SUM}$  of  $\delta D_{M,PRC,DJF}$ ,  $\delta D_{M,FT,DJF}$ , and  $\delta D_{M,SFC,DJF}$  closely resembles the respective  $S_{TOT}$ . This implies that in winter, feedbacks between the different fractionation processes in the model are small, which may be a result of the relatively small values of  $S_{ET,DJF}$  and  $S_{SC,DJF}$ . In summer, feedbacks between different fractionation processes are more relevant. For  $\delta D_{M,PRC,JJA}$ ,  $\delta D_{M,FT,JJA}$ , and  $\delta D_{M,SFC,JJA}$  the  $S_{TOT,JJA,SUM}$  is 18‰, 5‰, and 13‰ more positive than the value of  $S_{TOT,JJA}$ . For  $\delta D_{M,PRC,JJA}$  (Figure 9a) this results in a  $S_{TOT,JJA,SUM}$ , which is 30% higher than  $S_{TOT,JJA}$ . Following the definitions of sensitivities in Table 1 the difference between  $S_{TOT}$  and  $S_{TOT,SUM}$  can be written as

$$\begin{aligned}
 S_{TOT} - S_{TOT,SUM} &= S_{TOT} - S_R - S_{ET} - S_{SC} \\
 &= S_{TOT} - (S_{TOT} - S_{ET+SC}) - S_{ET} - S_{SC} \\
 &= S_{ET+SC} - (S_{ET} + S_{SC})
 \end{aligned} \tag{5}$$

According to the rearranged equation, the difference between  $S_{TOT}$  and  $S_{TOT,SUM}$  gives the deviation between the sum of sensitivities from model runs, in which either the effect of continental evapotranspiration or the effect of subcloud processes are turned off, and a model run, in which the effects of both processes are turned off. Hence, in our framework, the negative values of  $S_{TOT} - S_{TOT,SUM}$  imply a negative feedback between subcloud processes and continental evapotranspiration.

### 4.4. Attribution of Model Biases

Considering the findings from the sensitivity study, it is now possible to attribute the model biases of  $\delta D$  (thin dashed lines in Figure 9) more clearly to specific fractionation processes:

1. European  $\delta D_{M,PRC,DJF}$  closely agrees with observations (average difference of  $-4 \pm 1\%$ ). Given the small sensitivities to continental evapotranspiration and subcloud processes, this implies a reliable modeled  $\delta D$  of water vapor at the condensation level in winter. Furthermore, since the  $\delta D$  of water vapor around

- the condensation level is strongly controlled by the overall effect of rainout along an air parcel trajectory, the good agreement between  $\delta D_{M,PRC,DJF}$  and  $\delta D_{O,PRC,DJF}$  provides confidence in the model's ability to reproduce this process. However, compensating model uncertainty such as a high bias of  $\delta D_{M,vapor}$  and, for example, a too high condensation level with consequently lower  $\delta D$  cannot be completely ruled out in this study.
2. Because of a relatively large potential systematic uncertainty of the remote sensing measurements, it is not possible to accurately quantify the bias of  $\delta D_{M,FT}$ . However, the similar differences between  $\delta D_{M,FT}$  and  $\delta D_{O,FT}$  under cold and warm conditions imply a realistic temperature dependence of  $\delta D_{M,FT}$ . Together with (1), which for cold conditions implies a reliable representation of  $\delta D$  at the condensation level, this points to a reliable representation of  $\delta D$  at the condensation level also for warm conditions. A larger bias of  $\delta D_{M,FT,JJA}$ , however, would be possible in the case of different observational biases of  $\delta D_{O,FT,JJA}$  and  $\delta D_{O,FT,DJF}$  and could be caused, for example, by too strong vertical mixing in the model.
  3. In contrast to  $\delta D_{M,PRC,DJF}$ ,  $\delta D_{M,SFC,DJF}$  shows a high bias of  $+8 \pm 1\%$ . A likely reason for this bias is the larger sensitivity of  $\delta D_{M,SFC}$  to continental evapotranspiration, combined with uncertainty regarding model assumptions about isotope fractionation during surface evaporation at temperatures around the freezing point (Christner et al., 2017).
  4. European  $\delta D_{M,PRC,JJA}$  in summer is biased by  $+8 \pm 1\%$  ( $+16 \pm 2\%$  for Karlsruhe). Because the sensitivities of  $\delta D_{M,PRC,JJA}$  to the three different investigated fractionation processes are of similar magnitude, attributing this bias to a certain process would hardly be possible with a model-data comparison focusing only on precipitation. However, from the complementary multiplatform observations we conclude that  $\delta D_{M,SFC,JJA}$  agrees with  $\delta D_{O,SFC,JJA}$  within  $+2 \pm 1\%$ , ruling out significant uncertainty related to the  $\delta D$  of continental evapotranspiration under warm conditions as a reason for the bias of  $\delta D_{M,PRC,JJA}$ . In addition, finding (2) implies a reliable  $\delta D_{M,FT}$  around the condensation level under warm conditions. A likely explanation for the bias of  $\delta D_{M,PRC,JJA}$  is therefore an overestimation of the impact of subcloud processes in the model. As the parameterization of subcloud processes in models is relatively uncertain (Gedzelman & Arnold, 1994; Worden et al., 2007), an efficient way to reduce the bias of  $\delta D_{M,PRC,JJA}$  could be to tune the parameterization of subcloud processes to reduce  $S_{SC}$  of  $\delta D_{M,PRC,JJA}$  by 20% ( $-6\%$ ). The effect of this tuning on  $\delta D_{M,PRC,DJF}$  in winter,  $\delta D_{M,FT}$ , and  $\delta D_{M,SFC}$  would be relatively small because of their smaller  $S_{SC}$ .

## 5. Conclusions

In this study, we compared regional COSMO<sub>iso</sub> simulations of  $\delta D$  of water vapor in the lower free troposphere ( $\delta D_{M,FT}$ ),  $\delta D$  of near-surface water vapor ( $\delta D_{M,SFC}$ ), and  $\delta D$  in precipitation ( $\delta D_{M,PRC}$ ) with multiplatform  $\delta D$  observations from central Europe. The multiplatform observations include ground-based remote sensing observations, ground-based in situ measurements, and GNIP data. COSMO<sub>iso</sub> is able to reproduce the observed variations of  $\delta D_{FT}$ ,  $\delta D_{SFC}$ , and  $\delta D_{PRC}$  with  $R^2 = 0.73$ ,  $R^2 = 0.69$ , and  $R^2 = 0.67$ , respectively. We find the model biases of  $\delta D_{M,FT}$ ,  $\delta D_{M,SFC}$ , and  $\delta D_{M,PRC}$  to be almost independent of temperature and season, and small compared to the respective  $\delta D$  values. Both the good correlation and the small biases of  $\delta D$  imply a reliable representation of the most important isotope fractionation processes for different temperature regimes in the model over continental Europe.

By means of six sensitivity simulations, we disentangled the climatological impacts of rainout, continental evapotranspiration, and subcloud processes on  $\delta D_{M,FT}$ ,  $\delta D_{M,SFC}$ , and  $\delta D_{M,PRC}$  in central Europe. In this way, we identified a substantially different impact of these processes on the different types of  $\delta D$  observation. Because of these different impacts, misrepresentation of one of the investigated processes in the model would cause different biases when comparing the model to the different types of  $\delta D$  observations. For this reason, the good agreement between the modeled  $\delta D$  and the different types of  $\delta D$  observations rules out major coincidentally compensating model biases and further confirms a reliable model description of the fractionation processes that are most important for simulating  $\delta D_{M,FT}$ ,  $\delta D_{M,SFC}$ , and  $\delta D_{M,PRC}$ .

The impacts of the different fractionation processes on  $\delta D$  strongly depend on the season. In winter, when continental temperature gradients are largest, rainout is the controlling fractionation process for the investigated  $\delta D$  observations. For  $\delta D_{M,SFC,DJF}$ , the effect of rainout on  $\delta D$  is partly compensated by the effect of moisture uptake from continental evapotranspiration. Because of the high sensitivity of  $\delta D_{M,SFC,DJF}$  to continental evapotranspiration, COSMO<sub>iso</sub> could be used for investigating uncertain isotope fractionation processes during surface evaporation at temperatures around the freezing point (Christner et al., 2017) in future studies.



For summer, we found a smaller relative impact of rainout on  $\delta D$  than for cold conditions. For the investigated  $\delta D$  observations, the impact of rainout in summer is superimposed by the impact of continental evapotranspiration, which is on the same order of magnitude. In future studies, this strong signal from evapotranspiration could be used for investigating isotope fractionation during soil evaporation (e.g., Aemisegger et al., 2014). In addition to the impact of evapotranspiration, we find  $\delta D_{M,PRC,JJA}$  under warm condition to be very sensitive to subcloud processes, which is in line with earlier model experiments by Field et al. (2010) and Aemisegger et al. (2015). In combination the results point to an overestimation of these subcloud processes in COSMO<sub>iso</sub> by about 20%. This number, however, strongly depends on a potential model bias of  $\delta D$  at the condensation level. In order to further constrain such a model bias, very accurate observations of  $\delta D$  at the condensation level would be required. For this reason, more aircraft campaigns such as performed by Dyroff et al. (2015), Herman et al. (2014), and Sodemann et al. (2017) would be a very desirable and efficient measure for better constraining the observational biases of existing remote sensing measurements of  $\delta D$ .

Considering the different temperature dependencies of the investigated fractionation processes, the dominant control mechanisms of  $\delta D$  in precipitation over Europe strongly depends on climatic conditions. As also demonstrated by a sensitivity run with 3 K lower SST, showing a different response of  $\delta D$  in different regions and seasons, variations of isotope ratios in paleorecords from Europe may therefore not be interpreted only in terms of temperature changes. For present-day conditions, we successfully quantified the role of the most important fractionation processes determining isotope ratios in central Europe. In a similar way, the validated COSMO<sub>iso</sub> will be used for paleosimulations in future studies, allowing for a comprehensive interpretation of isotope records from Europe.

#### Acknowledgments

This study was funded by the German Climate Modeling Initiative (PalMod). F. A. acknowledges funding from the Swiss National Science Foundation (SNSF, grant P2EZP2\_155603) and hosting contributions from the Swedish research program Modeling the Regional and Global Earth system (MERGE). We thank MeteoSwiss and in particular Guy de Morsier for providing the code of TERRA stand-alone and technical assistance with the setup for the isotope implementation in TERRA. We thank Hui Tang for sharing his experience with isotope-enabled climate simulations, providing a routine for processing the ECHAM-wiso boundary data, and his helpful comments on the manuscript. The surface in situ and ground-based remote sensing water vapor isotopologue data have been produced within the framework of the project MUSICA, funded by the European Research Council under the European Community's Seventh Framework Programme (FP7/2007-2013/ERC grant agreement 256961). The observations of  $\delta D$  of near-surface water vapor are available as a supplement to Christner et al. (2017). For obtaining the observations of  $\delta D$  of free tropospheric water vapor please see Barthlott et al. (2017) or <http://www.imk-asf.kit.edu/english/2746.php>. For getting access to the simulations please contact the corresponding author.

#### References

- Aemisegger, F., Pfahl, S., Sodemann, H., Lehner, I., Seneviratne, S. I., & Wernli, H. (2014). Deuterium excess as a proxy for continental moisture recycling and plant transpiration. *Atmospheric Chemistry and Physics*, 14(8), 4029–4054. <https://doi.org/10.5194/acp-14-4029-2014>
- Aemisegger, F., Spiegel, J. K., Pfahl, S., Sodemann, H., Eugster, W., & Wernli, H. (2015). Isotope meteorology of cold front passages: A case study combining observations and modeling. *Geophysical Research Letters*, 42, 5652–5660. <https://doi.org/10.1002/2015GL063988>
- Aemisegger, F., Sturm, P., Graf, P., Sodemann, H., Pfahl, S., Knohl, A., et al. (2012). Measuring variations of  $\delta^{18}O$  and  $\delta^2H$  in atmospheric water vapour using two commercial laser-based spectrometers: An instrument characterisation study. *Atmospheric Measurement Techniques*, 5(7), 1491–1511. <https://doi.org/10.5194/amt-5-1491-2012>
- Araguas, L. A., Danesi, P., Froehlich, K., & Rozanski, K. (1996). Global monitoring of the isotopic composition of precipitation. *Journal of Radioanalytical and Nuclear Chemistry Articles*, 205(2), 189–200. <https://doi.org/10.1007/BF02039404>
- Barnes, C. J., & Allison, G. B. (1983). The distribution of deuterium and  $^{18}O$  in dry soils: 1. Theory. *Journal of Hydrology*, 60(1), 141–156.
- Barthlott, S., Schneider, M., Hase, F., Blumenstock, T., Kiel, M., Dubravica, D., et al. (2017). Tropospheric water vapour isotopologue data ( $H_2^{16}O$ ,  $H_2^{18}O$ , and  $HD^{16}O$ ) as obtained from NDACC/FTIR solar absorption spectra. *Earth System Science Data*, 9(1), 15–29. <https://doi.org/10.5194/essd-9-15-2017>
- Benetti, M., Reverdin, G., Pierre, C., Merlivat, L., Risi, C., Steen-Larsen, H. C., et al. (2014). Deuterium excess in marine water vapor: Dependency on relative humidity and surface wind speed during evaporation. *Journal of Geophysical Research: Atmospheres*, 119, 584–593. <https://doi.org/10.1002/2013JD020535>
- Blossey, P. N., Kuang, Z., & Roms, D. M. (2010). Isotopic composition of water in the tropical tropopause layer in cloud-resolving simulations of an idealized tropical circulation. *Journal of Geophysical Research*, 115, D24309. <https://doi.org/10.1029/2010JD014554>
- Boch, R., Cheng, H., Spötl, C., Edwards, R. L., Wang, X., & Häuselmann, P. (2011). NALPS: A precisely dated European climate record 120–60 ka. *Climate of the Past*, 7(4), 1247–1259. <https://doi.org/10.5194/cp-7-1247-2011>
- Christner, E., Kohler, M., & Schneider, M. (2017). The influence of snow sublimation and meltwater evaporation on  $\delta D$  of water vapor in the atmospheric boundary layer of central Europe. *Atmospheric Chemistry and Physics*, 17(2), 1207–1225. <https://doi.org/10.5194/acp-17-1207-2017>
- Coplen, T. B. (2011). Guidelines and recommended terms for expression of stable-isotope-ratio and gas-ratio measurement results. *Rapid Communications in Mass Spectrometry*, 25(17), 2538–2560. <https://doi.org/10.1002/rcm.5129>
- Craig, H., & Gordon, L. I. (1965). Deuterium and oxygen 18 variations in the ocean and marine atmosphere. *Stable isotopes in oceanographic studies and paleotemperatures*, 23. Pisa, Italy: Conoglio Nazionale delle Ricerche, Laboratorio di Geologia Nucleare.
- Dansgaard, W. (1964). Stable isotopes in precipitation. *Tellus*, 16(4), 436–468. <https://doi.org/10.1111/j.2153-3490.1964.tb00181.x>
- Dansgaard, W., Johnsen, S. J., Møller, J., & Langway, C. C. (1969). One thousand centuries of climatic record from camp century on the Greenland ice sheet. *Science*, 166(3903), 377–380. <https://doi.org/10.1126/science.166.3903.377>
- de Vries, J. J., & Simmers, I. (2002). Groundwater recharge: An overview of processes and challenges. *Hydrogeology Journal*, 10(1), 5–17. <https://doi.org/10.1007/s10040-001-0171-7>
- Doms, G., Forstner, J., Heise, E., Herzog, H. J., Raschendorfer, M., Reinhardt, T., et al. (1974). *A description of the nonhydrostatic regional model LM. Part II: Physical parameterization*. Offenbach, Germany: Deutscher Wetterdienst.
- Dongmann, G., Nürnberg, H. W., Förstel, H., & Wagener, K. (1974). On the enrichment of  $H_2^{18}O$  in the leaves of transpiring plants. *Radiation and Environmental Biophysics*, 11, 41–52.
- Dütsch, M. (2017). Stable water isotope fractionation processes in weather systems and their influence on isotopic variability on different time scales, Diss no. 23939 (PhD thesis), ETH Zurich.
- Dütsch, M., Pfahl, S., & Wernli, H. (2016). Drivers of  $\delta^2H$  variations in an idealized extratropical cyclone. *Geophysical Research Letters*, 43, 5401–5408. <https://doi.org/10.1002/2016GL068600>
- Dyroff, C., Sanati, S., Christner, E., Zahn, A., Balzer, M., Bouquet, H., et al. (2015). Airborne in situ vertical profiling of  $HDO/H_2^{16}O$  in the subtropical troposphere during the MUSICA remote sensing validation campaign. *Atmospheric Measurement Techniques*, 8(5), 2037–2049. <https://doi.org/10.5194/amt-8-2037-2015>



- Farquhar, G. D., & Cernusak, L. A. (2005). On the isotopic composition of leaf water in the non-steady state. *Functional Plant Biology*, *32*, 293–303.
- Field, R. D., Kim, D., LeGrande, A. N., Worden, J., Kelley, M., & Schmidt, G. A. (2014). Evaluating climate model performance in the tropics with retrievals of water isotopic composition from Aura TES. *Geophysical Research Letters*, *41*, 6030–6036. <https://doi.org/10.1002/2014GL060572>
- Field, R. D., Jones, D. B. A., & Brown, D. P. (2010). Effects of postcondensation exchange on the isotopic composition of water in the atmosphere. *Journal of Geophysical Research*, *115*, D24305. <https://doi.org/10.1029/2010JD014334>
- Frankenberg, C., Yoshimura, K., Warneke, T., Aben, I., Butz, A., Deutscher, N., et al. (2009). Dynamic processes governing lower-tropospheric HDO/H<sub>2</sub>O ratios as observed from space and ground. *Science*, *325*(5946), 1374–1377. <https://doi.org/10.1126/science.1173791>
- Friedman, I., Machta, L., & Soller, R. (1962). Water-vapor exchange between a water droplet and its environment. *Journal of Geophysical Research*, *67*(7), 2761–2766. <https://doi.org/10.1029/JZ067i007p02761>
- Gat, J. R. (1996). Oxygen and hydrogen isotopes in the hydrological cycle. *Annual Review of Earth and Planetary Sciences*, *24*(1), 225–262. <https://doi.org/10.1146/annurev.earth.24.1.225>
- Gedzelman, S. D., & Arnold, R. (1994). Modeling the isotopic composition of precipitation. *Journal of Geophysical Research*, *99*(D5), 10,455–10,471. <https://doi.org/10.1029/93JD03518>
- Harwood, K. G., Gillon, J. S., Roberts, A., & Griffiths, H. (1999). Determinants of isotopic coupling of CO<sub>2</sub> and water vapour within a Quercus petraea forest canopy. *Oecologia*, *119*(1), 109–119.
- Herman, R. L., Cherry, J. E., Young, J., Welker, J. M., Noone, D., Kulawik, S. S., et al. (2014). Aircraft validation of Aura Tropospheric Emission Spectrometer retrievals of HDO/H<sub>2</sub>O. *Atmospheric Measurement Techniques*, *7*(9), 3127–3138. <https://doi.org/10.5194/amt-7-3127-2014>
- Hoffmann, G., Werner, M., & Heimann, M. (1998). Water isotope module of the ECHAM atmospheric general circulation model: A study on timescales from days to several years. *Journal of Geophysical Research*, *103*(D14), 16,871–16,896. <https://doi.org/10.1029/98JD00423>
- IAEA (2009). *Reference sheet for VSMOW2 and SLAP2 international measurement standards*. Vienna: International Atomic Energy Agency.
- IAEA/WMO (2016). Retrieved from [http://www-naweb.iaea.org/naweb/ih/IHS\\_resources\\_gnip.html](http://www-naweb.iaea.org/naweb/ih/IHS_resources_gnip.html)
- Jacob, H., & Sonntag, C. (1991). An 8-year record of the seasonal variation of <sup>2</sup>H and <sup>18</sup>O in atmospheric water vapour and precipitation at Heidelberg, Germany. *Tellus B*, *43*(3), 291–300. <https://doi.org/10.1034/j.1600-0889.1991.t01-2-00003.x>
- Joussau, S., Sadourny, R., & Jouzel, J. (1984). A general circulation model of water isotope cycles in the atmosphere. *Nature*, *311*(5981), 24–29. <https://doi.org/10.1038/311024a0>
- Jouzel, J. (1986). Isotopes in cloud physics: Multi step and multi stage processes. In P. Fritz & J. Frontes (Eds.), *The terrestrial environment B* (Vol. 2, pp. 61–112). New York: Elsevier.
- Jouzel, J., & Merlivat, L. (1984). Deuterium and oxygen 18 in precipitation: Modeling of the isotopic effects during snow formation. *Journal of Geophysical Research*, *89*(D7), 11,749–11,757. <https://doi.org/10.1029/JD089iD07p11749>
- Jouzel, J., Hoffmann, G., Koster, R., & Masson, V. (2000). Water isotopes in precipitation. *Quaternary Science Reviews*, *19*(1-5), 363–379. [https://doi.org/10.1016/S0277-3791\(99\)00069-4](https://doi.org/10.1016/S0277-3791(99)00069-4)
- Majoube, M. (1971a). Fractionnement en oxygène-18 et en deutérium entre l'eau et sa vapeur. *Journal de Chimie Physique et de Physico*, *68*, 1423–1436.
- Majoube, M. (1971b). Fractionnement en oxygène-18 et en deutérium entre la glace et la vapeur d'eau. *Journal de Chimie Physique et de Physico*, *68*, 625–636.
- Mathieu, R., & Bariac, T. (1996). A numerical model for the simulation of stable isotope profiles in drying soils. *Journal of Geophysical Research*, *101*, 12,685–12,696. <https://doi.org/10.1029/96JD00223>
- Merlivat, L. (1978). Molecular diffusivities of H<sub>2</sub><sup>16</sup>O, HD<sup>16</sup>O, and H<sub>2</sub><sup>18</sup>O in gases. *Journal of Chemical Physics*, *69*, 2864–2871.
- Masson-Delmotte, V., Jouzel, J., Landais, A., Stievenard, M., Johnsen, S. J., White, J. W. C., et al. (2005). GRIP deuterium excess reveals rapid and orbital-scale changes in Greenland moisture origin. *Science*, *309*(5731), 118–121. <https://doi.org/10.1126/science.1108575>
- Noone, D., Galewsky, J., Sharp, Z. D., Worden, J., Barnes, J., Baer, D., et al. (2011). Properties of air mass mixing and humidity in the subtropics from measurements of the D/H isotope ratio of water vapor at the Mauna Loa Observatory. *Journal of Geophysical Research*, *116*, D22113. <https://doi.org/10.1029/2011JD015773>
- Pfahl, S., & Wernli, H. (2009). Lagrangian simulations of stable isotopes in water vapor: An evaluation of nonequilibrium fractionation in the Craig-Gordon model. *Journal of Geophysical Research*, *114*, D20108. <https://doi.org/10.1029/2009JD012054>
- Pfahl, S., Wernli, H., & Yoshimura, K. (2012). The isotopic composition of precipitation from a winter storm—A case study with the limited-area model COSMOiso. *Atmospheric Chemistry and Physics*, *12*(3), 1629–1648. <https://doi.org/10.5194/acp-12-1629-2012>
- Riley, W. J., Still, C. J., Torn, M. S., & Berry, J. A. (2002). A mechanistic model of H<sub>2</sub><sup>18</sup>O and C<sup>18</sup>OO fluxes between ecosystems and the atmosphere: Model description and sensitivity analyses. *Global Biogeochemical Cycles*, *16*(4), 1095. <https://doi.org/10.1029/2002GB001878>
- Richards, L. A. (1931). Capillary conduction of liquids through porous mediums. *Physics*, *1*, 318–333. <https://doi.org/10.1063/1.1745010>
- Risi, C., Noone, D., Worden, J., Frankenberg, C., Stiller, G., Kiefer, M., et al. (2012a). Process-evaluation of tropospheric humidity simulated by general circulation models using water vapor isotopologues: 1. Comparison between models and observations. *Journal of Geophysical Research*, *117*, D05303. <https://doi.org/10.1029/2011JD016621>
- Risi, C., Noone, D., Worden, J., Frankenberg, C., Stiller, G., Kiefer, M., et al. (2012b). Process-evaluation of tropospheric humidity simulated by general circulation models using water vapor isotopic observations: 2. Using isotopic diagnostics to understand the mid and upper tropospheric moist bias in the tropics and subtropics. *Journal of Geophysical Research*, *117*, D05304. <https://doi.org/10.1029/2011JD016623>
- Risi, C., Ogee, J., Bony, S., Bariac, T., Raz Yaseef, N., Wingate, L., et al. (2016). The water isotopic version of the land-surface model ORCHIDEE: Implementation, evaluation, sensitivity to hydrological parameters. *Hydrology: Current Research*, *7*(4), 2157–7587. <https://doi.org/10.4172/2157-7587.1000258>
- Rockel, B., Will, A., & Hense, A. (2008). The regional climate model COSMO-CLM (CCLM). *Meteorologische Zeitschrift*, *17*(4), 347–348. <https://doi.org/10.1127/0941-2948/2008/0309>
- Rokotyan, N. V., Zakharov, V. I., Gribov, K. G., Schneider, M., Bréon, F., et al. (2014). A posteriori calculation of δ<sup>18</sup>O and δD in atmospheric water vapour from ground-based near-infrared FTIR retrievals of H<sub>2</sub><sup>16</sup>O, H<sub>2</sub><sup>18</sup>O, and HD<sup>16</sup>O. *Atmospheric Measurement Techniques*, *7*(8), 2567–2580. <https://doi.org/10.5194/amt-7-2567-2014>
- Schneider, M., & Hase, F. (2011). Optimal estimation of tropospheric H<sub>2</sub>O and δD with IASI/METOP. *Atmospheric Chemistry and Physics*, *11*(21), 11,207–11,220. <https://doi.org/10.5194/acp-11-11207-2011>

- Schneider, M., Barthlott, S., Hase, F., González, Y., Yoshimura, K., García, O. E., et al. (2012). Ground-based remote sensing of tropospheric water vapour isotopologues within the project MUSICA. *Atmospheric Measurement Techniques*, 5(12), 3007–3027. <https://doi.org/10.5194/amt-5-3007-2012>
- Schneider, M., Borger, C., Wiegeler, A., Hase, F., García, O. E., Sepúlveda, E., et al. (2017). MUSICA MetOp/IASI (H<sub>2</sub>O, δD) pair retrieval simulations for validating tropospheric moisture pathways in atmospheric models. *Atmospheric Measurement Techniques*, 10(2), 507–525. <https://doi.org/10.5194/amt-10-507-2017>
- Schneider, M., Wiegeler, A., Barthlott, S., González, Y., Christner, E., Dyroff, C., et al. (2016). Accomplishments of the MUSICA project to provide accurate, long-term, global and high-resolution observations of tropospheric {H<sub>2</sub>O, δD} pairs: a review. *Atmospheric Measurement Techniques*, 9(7), 2845–2875. <https://doi.org/10.5194/amt-9-2845-2016>
- Schoch-Fischer, H., Rozanski, K., Jacob, H., Sonntag, C., Jouzel, J., Östlund, G., & Geyh, M. A. (1983). Hydrometeorological factors controlling the time variation of D, <sup>18</sup>O and <sup>3</sup>H in atmospheric water vapour and precipitation in the northern westwind belt. In IAEA (Ed.), *Isotope Hydrology* (pp. 3–30). Vienna: IAEA.
- Schrodin, R., & Heise, E. (2001). The multi-layer version of the DWD soil model TERRA-LM. *Consortium for Small-Scale Modelling (COSMO) Tech. Rep.*, 2, 16.
- Sodemann, H., & Zubler, E. (2010). Seasonal and inter-annual variability of the moisture sources for Alpine precipitation during 1995–2002. *International Journal of Climatology*, 30, 947–961. <https://doi.org/10.1002/joc.1932>
- Sodemann, H., Aemisegger, F., Pfahl, S., Bitter, M., Corsmeier, U., Feuerle, T., et al. (2017). The stable isotopic composition of water vapour above Corsica during the HyMeX SOP1 campaign: Insight into vertical mixing processes from lower-tropospheric survey flights. *Atmospheric Chemistry and Physics*, 17, 6125–6151. <https://doi.org/10.5194/acp-17-6125-2017>
- Steen-Larsen, H. C., Sveinbjörnsdóttir, A. E., Peters, A. J., Masson-Delmotte, V., Guishard, M. P., Hsiao, G., et al. (2014). Climatic controls on water vapor deuterium excess in the marine boundary layer of the North Atlantic based on 500 days of in situ, continuous measurements. *Atmospheric Chemistry and Physics*, 14(15), 7741–7756. <https://doi.org/10.5194/acp-14-7741-2014>
- Steppeler, J., Doms, G., Schaettler, U., Bitzer, H. W., Gassmann, A., Damrath, U., et al. (2003). Meso-gamma scale forecasts using the nonhydrostatic model LM. *Meteorology and Atmospheric Physics*, 82(1-4), 75–96. <https://doi.org/10.1007/s00703-001-0592-9>
- Stewart, M. K. (1975). Stable isotope fractionation due to evaporation and isotopic exchange of falling waterdrops: Applications to atmospheric processes and evaporation of lakes. *Journal of Geophysical Research*, 80(9), 1133–1146. <https://doi.org/10.1029/JC080i009p01133>
- Taylor, C. B. (1984). Vertical distribution of deuterium in atmospheric water vapour: Problems in application to assess atmospheric condensation models. *Tellus B*, 36B(1), 67–70. <https://doi.org/10.1111/j.1600-0889.1984.tb00053.x>
- von Storch, H., Langenberg, H., & Feser, F. (2000). A spectral nudging technique for dynamical downscaling purposes. *Monthly Weather Review*, 128(10), 3664–3673. [https://doi.org/10.1175/1520-0493\(2000\)128<3664:ASNTFD>2.0.CO;2](https://doi.org/10.1175/1520-0493(2000)128<3664:ASNTFD>2.0.CO;2)
- Wang, L., Good, S. P., Caylor, K. K., & Cernusak, L. A. (2012). Direct quantification of leaf transpiration isotopic composition. *Agricultural and Forest Meteorology*, 154, 127–135.
- Wang, Y. J. (2001). A high-resolution absolute-dated late pleistocene monsoon record from Hulu Cave, China. *Science*, 294(5550), 2345–2348. <https://doi.org/10.1126/science.1064618>
- Washburn, E., & Smith, E. (1934). The isotopic fractionation of water by physiological processes. *Science*, 79, 188–189.
- Werner, M., Langebroek, P. M., Carlsen, T., Herold, M., & Lohmann, G. (2011). Stable water isotopes in the ECHAM5 general circulation model: Toward high-resolution isotope modeling on a global scale. *Journal of Geophysical Research*, 116, D15109. <https://doi.org/10.1029/2011JD015681>
- Worden, J., Bowman, K., Noone, D., Beer, R., Clough, S., Eldering, A., et al. (2006). Tropospheric Emission Spectrometer observations of the tropospheric HDO/H<sub>2</sub>O ratio: Estimation approach and characterization. *Journal of Geophysical Research*, 111, D16309. <https://doi.org/10.1029/2005JD006606>
- Worden, J., Noone, D., Bowman, K., Beer, R., Eldering, A., Fisher, B., et al. (2007). Importance of rain evaporation and continental convection in the tropical water cycle. *Nature*, 445(7127), 528–532. <https://doi.org/10.1038/nature05508>
- Yoshimura, K. (2015). Stable water isotopes in climatology, meteorology, and hydrology: A review. *Journal of the Meteorological Society of Japan. Ser. II*, 93(5), 513–533. <https://doi.org/10.2151/jmsj.2015-036>
- Zhang, S., Wen, X., Wang, J., Yu, G., & Sun, X. (2010). The use of stable isotopes to partition evapotranspiration fluxes into evaporation and transpiration. *Acta Ecologica Sinica*, 30(4), 201–209. <https://doi.org/10.1016/j.chnaes.2010.06.003>